



# Design, synthesis and biological evaluation of novel 2-(4-(1*H*-indazol-6-yl)-1*H*-pyrazol-1-yl)acetamide derivatives as potent VEGFR-2 inhibitors



Xing-Rong Wang, Shuai Wang, Wen-Bo Li, Kai-Yan Xu, Xue-Peng Qiao, Xue-Li Jing, Zi-Xiao Wang, Chang-jiang Yang, Shi-Wu Chen\*

School of Pharmacy, Lanzhou University, Lanzhou, 730000, China

## ARTICLE INFO

### Article history:

Received 5 November 2020

Received in revised form

28 December 2020

Accepted 10 January 2021

Available online 18 January 2021

### Keywords:

VEGFR-2

Indazole

Anti-gastric cancer

Apoptosis

Anti-angiogenesis

## ABSTRACT

Vascular endothelial growth factor-2 (VEGFR-2) plays a pivotal role in tumor angiogenesis. Herein, a library of novel 2-(4-(1*H*-indazol-6-yl)-1*H*-pyrazol-1-yl)acetamide derivatives were designed and synthesized as VEGFR-2 inhibitors based on scaffold hopping strategy. These compounds exhibited the excellent inhibitory in both VEGFR-2 and tumor cells proliferation. Especially, compound **W13** possessed potent VEGFR-2 inhibition with  $IC_{50} = 1.6$  nM and anti-proliferation against HGC-27 tumor cells with  $IC_{50} = 0.36 \pm 0.11$   $\mu$ M, as well as less toxicity against normal GES-1 cells with  $IC_{50} = 187.46 \pm 10.13$   $\mu$ M. Moreover, **W13** obviously inhibited colony formation, migration and invasion of HGC-27 cells by adjusting the expression of MMP-9 and E-cadherin, and induced HGC-27 cells apoptosis by increasing ROS production and regulating the expression of apoptotic proteins. Furthermore, **W13** blocked the PI3K-Akt-mTOR signaling pathway in HGC-27 cells. In addition, anti-angiogenesis of **W13** was proved by inhibiting tube formation and the expression of p-VEGFR-2 in HUVEC cells. All the results demonstrated that **W13** could be developing as a promising anticancer agent for gastric cancer therapy.

© 2021 Elsevier Masson SAS. All rights reserved.

## 1. Introduction

Angiogenesis plays an important role in tumor growth and metastasis, and has been widely studied in a variety of clinical pathological diseases including cancer, rheumatoid arthritis, diabetic neuropathy and psoriasis [1,2]. Vascular endothelial growth factor-2 (VEGFR-2), as the most prominent angiogenic factor, belongs to type III receptor tyrosine kinase and is highly activated on vascular endothelial cells after combining with VEGF secreted by tumor cells [3]. Continuously active VEGFR-2 leads to the construction of tumor blood vessel network, thereby providing nutrition and oxygen to tumor tissue and enhancing tumor proliferation, invasion and metastasis. More recent studies have confirmed that VEGFR-2 is over-expressed in liver, gastric, colon, lung and breast cancer [4–7].

Over the past decades, many effective small molecule VEGFR-2 tyrosine kinase inhibitors have been approved by the USA-FDA and achieved satisfactory clinical results [8–11], which can be

classified into type I and type II according to the trend of Asp-Phe-Gly (DFG) conservative motif in the kinase [12]. Type I inhibitors bind to the ATP binding site with DFG-in “active” conformation, such as Axitinib (I), Sunitinib (II) and Pazopanib (III) [13–15]. In contrast, type II inhibitors conduct a DFG-out “inactive” conformation at the ATP binding site, including Linifanib (IV), Apatinib (V) and Sorafenib (VI) [16–18] (Fig. 1). The latter can not only occupy the hydrophobic “back pocket” of kinase, it also enhance the affinity and specificity of protein-ligand complex, resulting in better selectivity and more extensive research on type II inhibitors [12].

Sorafenib (Nexavar) is an oral multi-target tyrosine kinase inhibitor with anti-angiogenic and anti-proliferative effects, having been approved for the treatment of metastatic renal cell carcinoma (mRCC) and hepatocellular carcinoma (HCC) in the first-line setting [19,20]. Multiple clinical trials have shown that sorafenib can effectively improve the progression-free survival rate and overall survival rate of cancer patients [21–23]. However, the problems of sorafenib have appeared in clinical medications, such as acquire resistance, cardiovascular toxicity and acute elevated blood pressure [24–26]. Besides, sorafenib performs low oral bioavailability (about 8.43%), poor water solubility, high protein binding rate (99.5%) and a long half-life of 25–48 h [27]. Hence, developments of

\* Corresponding author.

E-mail address: [chenshw@lzu.edu.cn](mailto:chenshw@lzu.edu.cn) (S.-W. Chen).

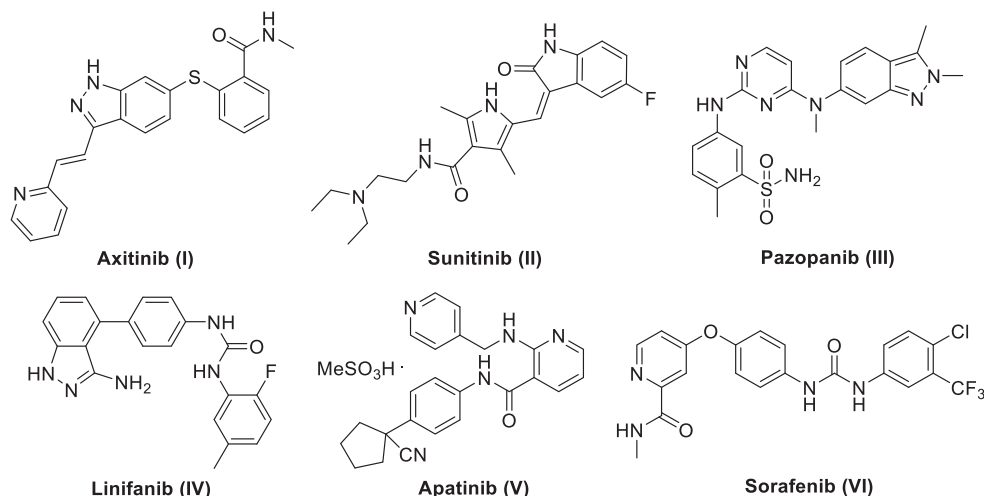


Fig. 1. VEGFR-2/multitargeted inhibitors approved for clinical use.

more efficiency and less toxicity VEGFR-2 inhibitors basing sorafenib make it more meaningful for medicinal chemists.

Indazoles are widely used in anticancer, antidiabetic, analgesic, antidepressant and neurodegenerative disorders due to excellent pharmacological activity [28]. Recently, Liu et al. reported an indazole VEGFR-2 inhibitor based on the Axitinib which showed excellent pharmacokinetic properties and safety [29]. Therefore, we first designed and synthesized 3-amino-1*H*-indazole **W1** via the scaffold hopping strategy basing three-dimensional conformation, and the preliminary VEGFR-2 activity indicated that **W1** showed a moderate inhibition with an  $IC_{50}$  of 892 nM, consistent with the docking result and could be carried out as a lead compound for later structure optimization and structure-activity relationship (SAR) discussion (Fig. 2). Moreover, the most potent compound **W13** was selected to identify the preliminary action mechanisms. The results provided a new chemical tool or potent candidate for gastric cancer therapy.

## 2. Results and discussions

### 2.1. Design strategy

The molecular framework is not only the key to maintaining activity, but also the basis for innovative drug design. Scaffold hopping strategy basing three-dimensional conformation refers to the use of an overall design strategy to find a scaffold with the same three-dimensional orientation and conformation as the active compound, rather than a part of the chemical group. Structural analysis of the clinical type II VEGFR-2 inhibitors by molecular

docking found that they comprise five parts: the hinge binding, solvent exposure area, linker, hydrogen binding and tail inserting into hydrophobic back pocket. Additionally, the X-ray crystallographic structures of VEGFR-2 (PDB ID: 3EWH [30]) in DFG-out inactive conformation was selected and downloaded from RCSB Protein Data Bank. The bond angle formed by the oxygen atom in the sorafenib extends the arylurea side chain into the hydrophobic back pocket. This non-coplanar conformation of the pyridine and benzene ring is the basis for maintaining activity.

Based on the observations described above, we regarded the pyridine-oxy-phenyl of sorafenib as a whole, combined with the glide-docking experiments, and found a 6-(1*H*-pyrazol-4-yl)-1*H*-indazol-3-amine scaffold that could be basically consistent with the three-dimensional conformation of sorafenib (Fig. 3A and B). In addition, it was found that the hydrogen atom at  $N^1$  and the  $N^2$  atom of indazole core formed stable hydrogen bonding with Glu 917 and Cys 919, respectively. Besides, the  $N^2$  atom of pyrazole formed additional hydrogen bonding with Lys 868. Based on this scaffold, we first designed and synthesized compound **W1** by introducing the pyridine ring to solvent exposure area and inserting a trifluoromethyl phenyl to hydrophobic back pocket through the acetamide group, which formed key hydrogen bonding with the side chain of Glu 885 in the  $\alpha$ C helix and Asp 1046 in the conserved DFG motif, stabilizing VEGFR-2 in DFG-out inactive conformation and resembling to sorafenib (Fig. 3C). Furthermore, replacing urea with acetamide could improve molecular water solubility.

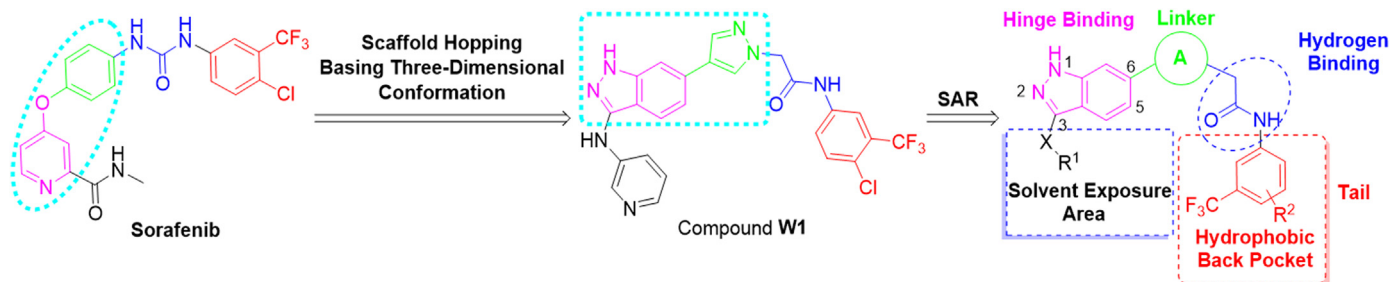
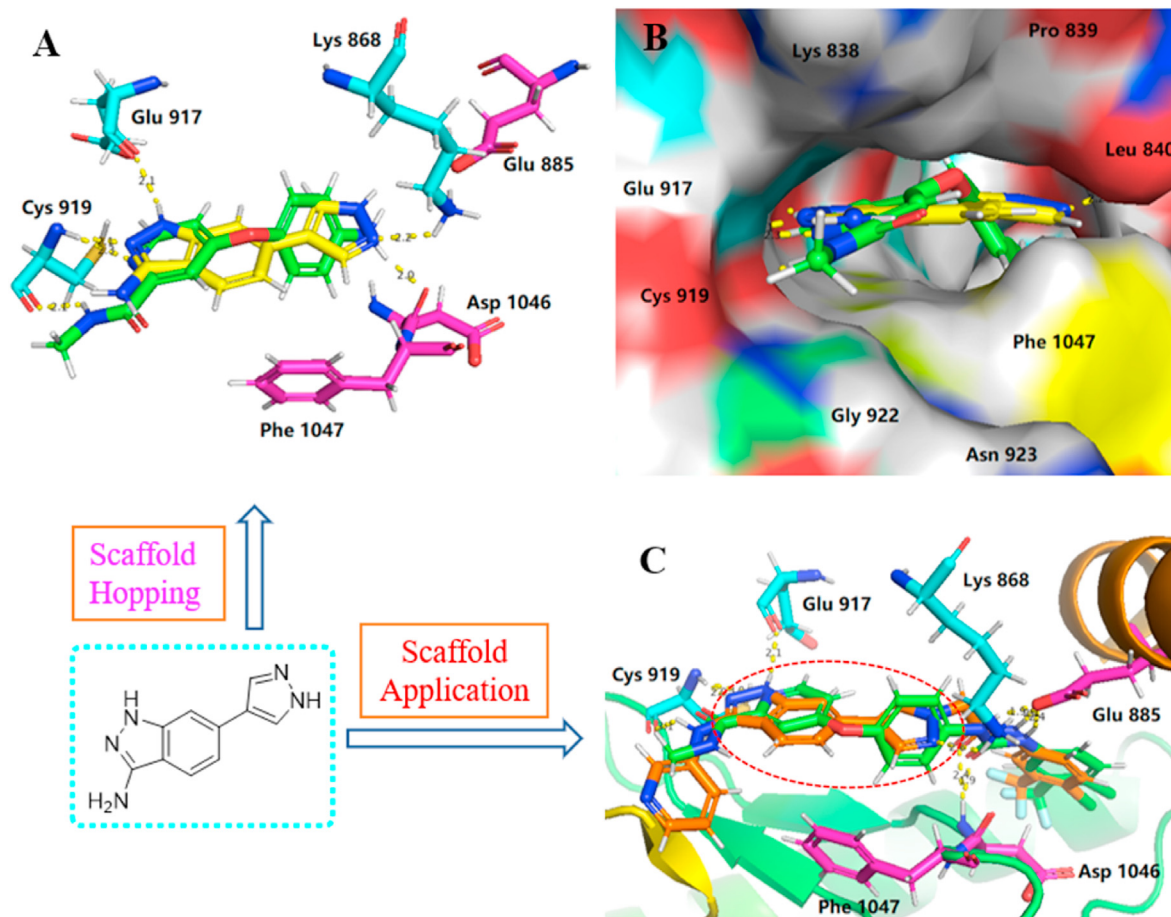


Fig. 2. The rationally design of target compounds.



**Fig. 3.** Docking models of novel 1H-indazoles VEGFR-2 inhibitors. (A, B) Docking models of 6-(1H-pyrazol-4-yl)-1H-indazol-3-amine scaffold (yellow) and sorafenib scaffold (green), and overlap of the proposed surface binding mode (PDB code: 3EWH); (C) Docking models of compound **W1** (orange) and sorafenib (green) (PDB code: 3EWH); Yellow dashed lines indicate the hydrogen bonds and important active site residues were labeled and colored with cyan and magenta.

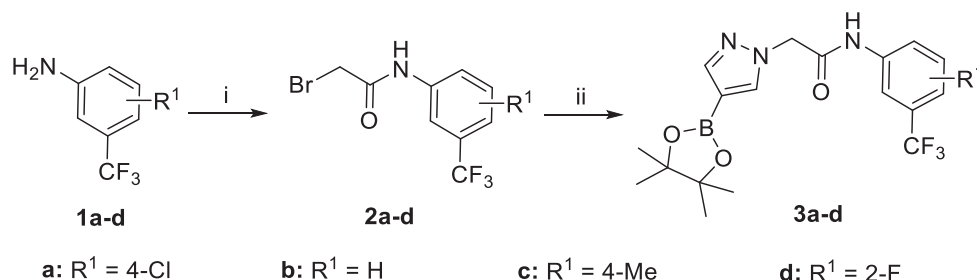
## 2.2. Chemistry

Above all, the key intermediates **3a–d** were synthesized as described in Scheme 1. Specially, commercially available 3-trifluoromethylaniline derivatives **1a–d** were reacted with bromoacetyl bromide to obtain 2-bromo-*N*-(3-(trifluoromethyl)phenyl) acetamide derivatives **2a–d**, which were underwent a nucleophilic substitution with 4-(4,4,5,5-tetramethyl-1,3,2-dioxaborolan-2-yl)-1H-pyrazole to give **3a–d**.

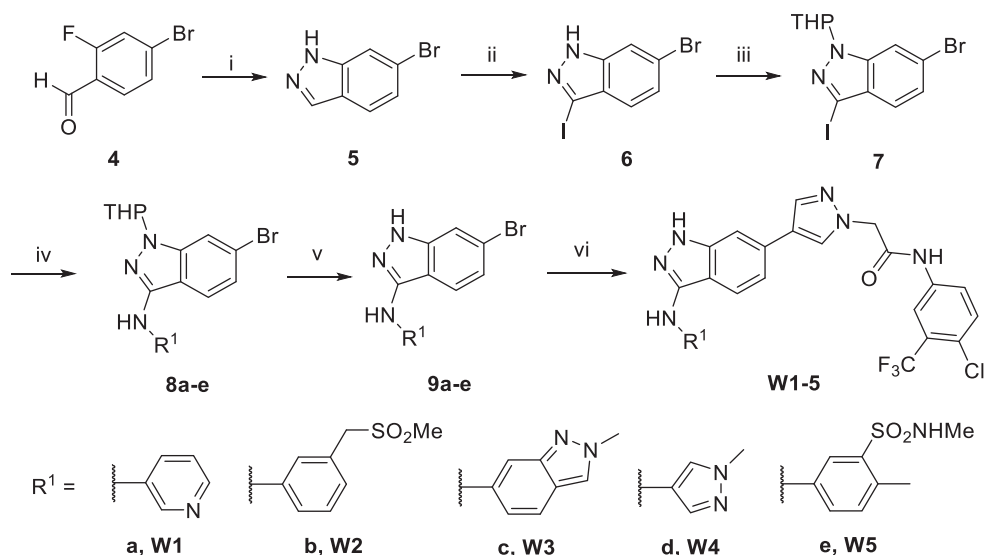
The synthesis of target compounds **W1–5** was outlined in Scheme 2. Firstly, coupling of 4-bromo-2-fluorobenzaldehyde (**4**) and hydrazine gave 6-bromo-1H-indazole (**5**), which followed a nucleophilic substitution and an addition reaction with 3,4-

dihydro-2H-pyran to provide *N*-protected indazole (**7**). Following, through Buchwald-Hartwig reaction of **7** with different aromatic amines, 3-arylamine substituted indazoles **8a–e** were obtained, which then removed pyran protecting group by using trifluoroacetic acid to give 6-bromo-3-arylamine-1H-indazoles **9a–e**. Lastly, Suzuki coupling reaction of **9a–e** and **3a** under the catalysis of Pd(dppf)Cl<sub>2</sub>·CH<sub>2</sub>Cl<sub>2</sub> afforded **W1–5** [31].

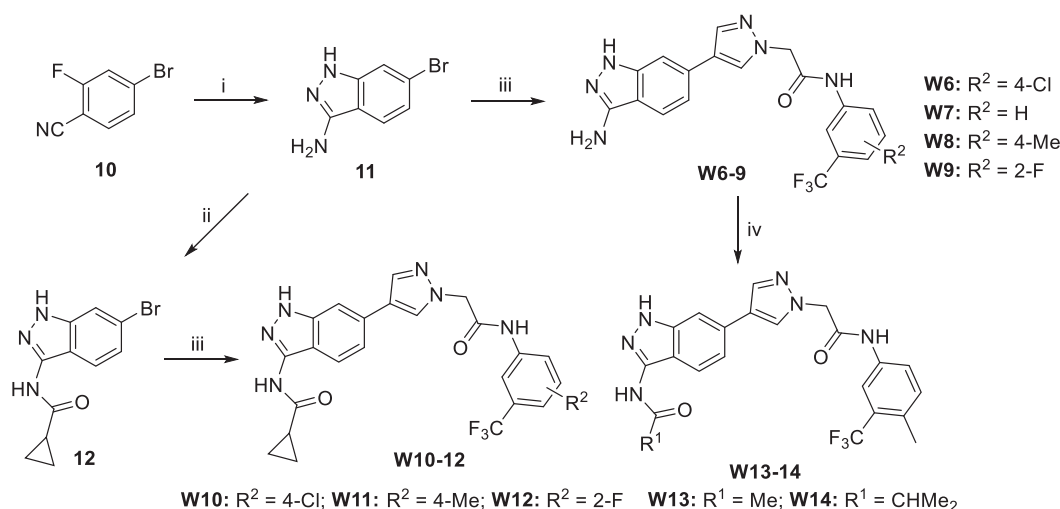
The target compounds **W6–14** were synthesized as summarized in Scheme 3. Coupling of 4-bromo-2-fluorobenzonitrile (**10**) and hydrazine gave 6-bromo-1H-indazole-3-amine (**11**), which was then condensed with cyclopropane carbonyl chloride to give cyclopropanecarboxamide (**12**) [32]. Intermediate **11** or **12** was reacted with intermediates **3a–d** via palladium catalyzed Suzuki



**Scheme 1.** Reagents and conditions: (i) Bromoacetyl bromide, Et<sub>3</sub>N, CH<sub>2</sub>Cl<sub>2</sub>, rt, 3 h; (ii) 4-(4,4,5,5-tetramethyl-1,3,2-dioxaborolan-2-yl)-1H-pyrazole, KI, Cs<sub>2</sub>CO<sub>3</sub>, CH<sub>3</sub>CN, reflux, 4 h.



**Scheme 2.** Reagents and conditions: (i) 80%  $\text{NH}_2\text{NH}_2 \cdot \text{H}_2\text{O}$ , p-TsOH, EtOH, 100–130 °C, 12 h; (ii)  $\text{I}_2$ , KOH, DMF, 0 °C–rt, 4 h; (iii) 3,4-dihydro-2H-pyran, p-TsOH, THF, reflux, 7 h; (iv) relative amine,  $\text{Pd}(\text{OAc})_2$ , xantphos,  $\text{Cs}_2\text{CO}_3$ , dry 1,4-dioxane, 100 °C, 3 h; (v) TFA,  $\text{CH}_2\text{Cl}_2$ , 0 °C–rt, 4 h; (vi) compound **3a**,  $\text{Pd}(\text{dppf})\text{Cl}_2 \cdot \text{CH}_2\text{Cl}_2$ , 2 M  $\text{Na}_2\text{CO}_3$  aq, 1,4-dioxane, 100 °C, 3 h.



**Scheme 3.** Reagents and conditions: (i) 80%  $\text{NH}_2\text{NH}_2 \cdot \text{H}_2\text{O}$ , *n*-BuOH, 120 °C, 4 h; (ii) cyclopropane carbonyl chloride, pyridine, 0 °C, 4 h; (iii) compounds **3a–3d**,  $\text{Pd}(\text{dppf})\text{Cl}_2 \cdot \text{CH}_2\text{Cl}_2$ , 2 M  $\text{Na}_2\text{CO}_3$  aq, 1,4-dioxane, 100 °C, 3 h; (iv) compound **W8**, acetyl chloride (for **W13**) or isobutyryl chloride (for **W14**), DIEA, THF, rt, 18 h; then 2 M  $\text{K}_2\text{CO}_3$  aq, MeOH-THF (1:1), rt, 1 h.

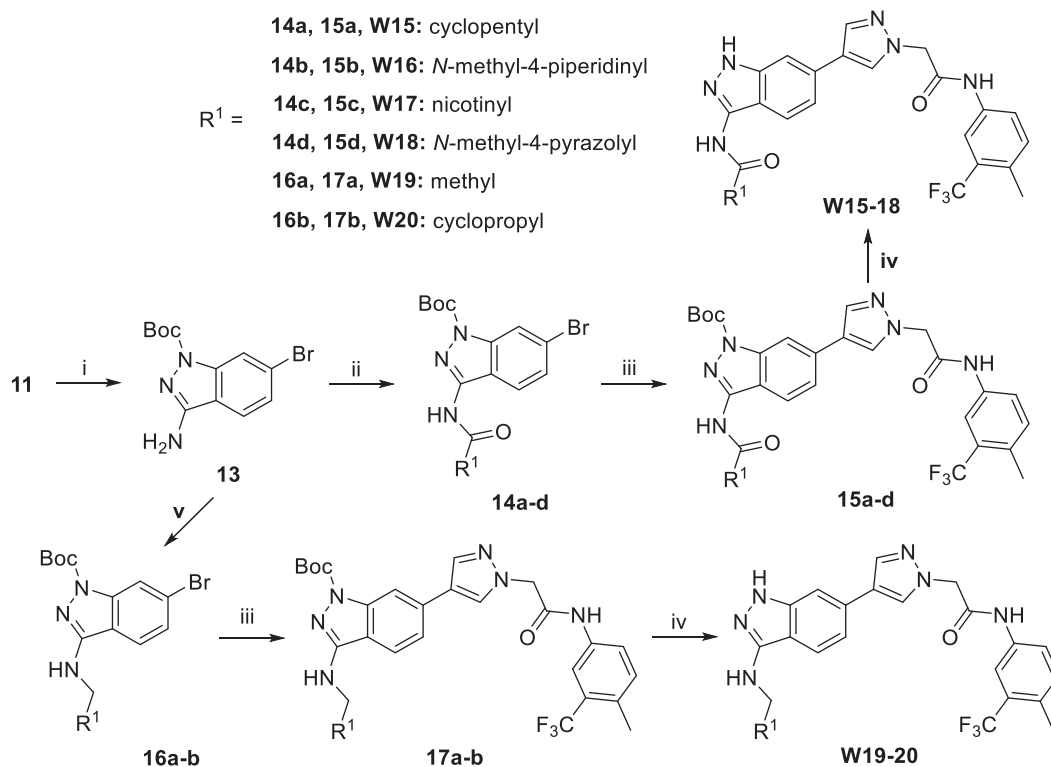
coupling reaction to obtain **W6–12**. Furthermore, compound **W8** was directly converted into **W13–14** by reacting with acetyl chloride or isobutyryl chloride in suitable 2 M  $\text{K}_2\text{CO}_3$  solution.

The target compounds **W15–20** were obtained according to the methods summarized in [Scheme 4](#). The  $\text{N}^1$  atom of 6-bromo-1H-indazole-3-amine (**11**) was selectively protected with di-*tert*-butyl pyrocarbonate ( $\text{Boc}_2\text{O}$ ) to provide compound **13** [33]. On the one hand, the exposed  $\text{NH}_2$  at C3 of **13** was coupled with various acid chloride to give compounds **14a–d** [34]. On the other hand, it was reacted with the corresponding aldehyde to form an alkyl substituted intermediates **16a–b** [35] in the presence of  $\text{NaBH}(\text{OAc})_3$ . Following, a Suzuki coupling reaction between **14a–d** or **16a–b** and compound **3c** were conducted, and then removed *N*-Boc group with trifluoroacetic acid to give target compounds **W15–20**, respectively.

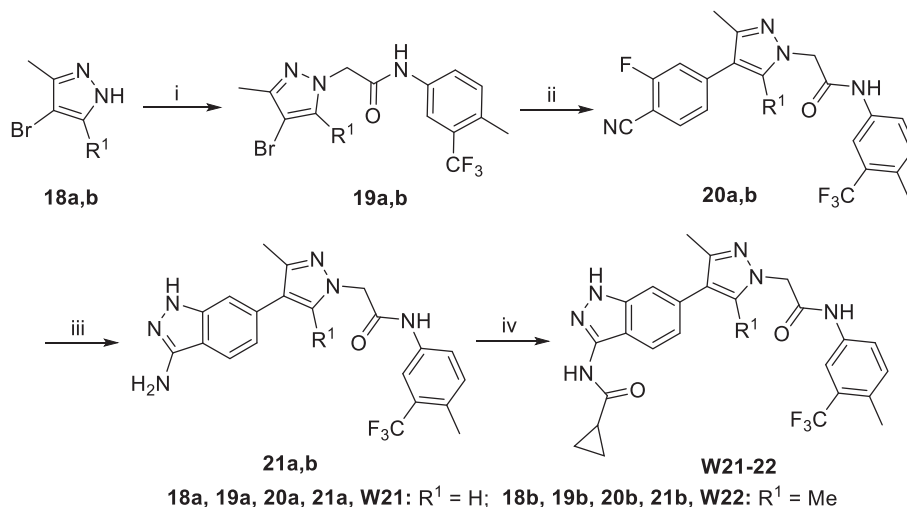
The target compounds **W21–22** were obtained according to the

method summarized in [Scheme 5](#). Commercial 4-bromomethylpyrazole derivatives **18a–b** were converted into **19a–b** by reacting with compound **2c**, which underwent a Suzuki coupling reaction to give **20a–b**, and then condensed with hydrazine to obtain **21a–b**. Ultimately, intermediates **21a–b** were directly converted into **W21–22** by reacting with cyclopropane carbonyl chloride.

The synthesis of target compounds **W23–25** was outlined in [Scheme 6](#). Commercially material 2-(5-bromothiophen-2-yl)acetic acid **22** or bromophenylacetic acid **25a–b** were condensed with 4-methyl-3-(trifluoromethyl) aniline using dicyclohexylcarbodiimide (DCC) and 1-hydroxybenzotriazole (HOBT) as coupling agents to afford compounds **23** or **26a–b**, which were converted into borate-substituted derivatives **24** or **27a–b** [36] via  $\text{Pd}(\text{dppf})\text{Cl}_2$  catalyzed. Finally, it was reacted with intermediate **12** by Suzuki coupling reaction to obtain **W23–25**.



**Scheme 4.** Reagents and conditions: (i)  $(\text{Boc})_2\text{O}$ , DMAP, THF,  $0^\circ\text{C}$ –rt, 3 h; (ii) Acid chloride, pyridine,  $\text{CH}_2\text{Cl}_2$ , rt or reflux, 3 h; (iii) compound **3c**,  $\text{Pd}(\text{dppf})\text{Cl}_2 \cdot \text{CH}_2\text{Cl}_2$ , 2 M  $\text{Na}_2\text{CO}_3$  aq, 1,4-dioxane,  $100^\circ\text{C}$ , 3 h; (iv) TFA,  $\text{CH}_2\text{Cl}_2$ ,  $0^\circ\text{C}$ –rt, 4 h; (v) acetaldehyde (for **16a**) or cyclopropane carboxaldehyde (for **16b**),  $\text{NaBH}(\text{OAc})_3$ , acetic acid, DME, rt, 18 h.



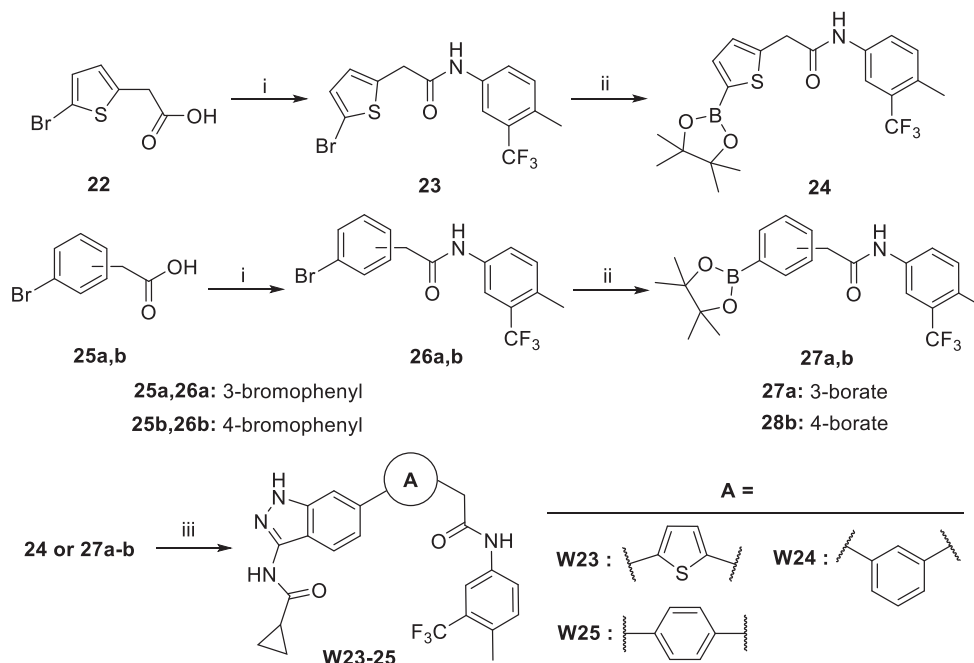
**Scheme 5.** Reagents and conditions: (i) compound **2c**, KI,  $\text{Cs}_2\text{CO}_3$ , acetonitrile, reflux, 4 h; (ii) 2-fluoro-4-(4,4,5,5-tetramethyl-1,3,2-dioxaborolan-2-yl)benzotrile,  $\text{Pd}(\text{dppf})\text{Cl}_2 \cdot \text{CH}_2\text{Cl}_2$ , 2 M  $\text{Na}_2\text{CO}_3$  aq, 1,4-dioxane,  $100^\circ\text{C}$ , 3 h; (iii) 80%  $\text{NH}_2\text{NH}_2 \cdot \text{H}_2\text{O}$ , *n*-BuOH,  $125^\circ\text{C}$ , 3 h; (iv) cyclopropane carbonyl chloride, DIEA, THF, rt, 18 h; then 2 M  $\text{K}_2\text{CO}_3$  aq, MeOH-THF (1:1), rt, 1 h.

The target compound **W26** was prepared as outlined in [Scheme 7](#). 2-Bromo-*N*-(4-methyl-3-(trifluoromethyl)phenyl)acetamide **2c** was treated with sodium azide to give **28**, which was coupled with 4-ethynyl-2-fluorobenzotrile [37] to obtain triazole derivative **29** via Click reaction [38], and reacted with hydrazine to obtain the indazole core and further converted into **W26** as described in synthesis of **W13**.

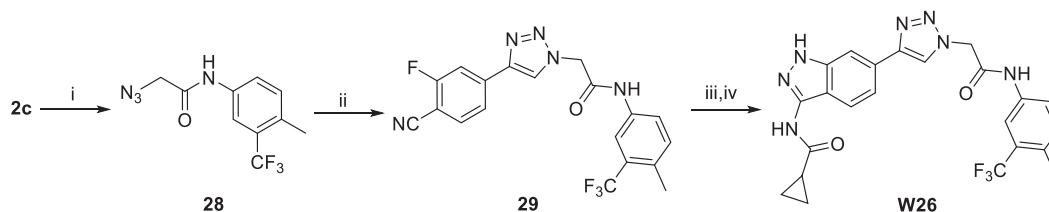
### 2.3. Biological evaluation

#### 2.3.1. *In vitro* VEGFR-2 inhibitory assay

All the synthesized target compounds **W1–26** were evaluated for their inhibitory activities against VEGFR-2 by Caliper Mobility-Shift Assay using sorafenib as a positive control. As shown in [Table 1](#), all the target compounds exhibited more than 53.8% inhibition at  $1\ \mu\text{M}$  against VEGFR-2. Initially, based on the lead compound **W1**, we replaced the 3-pyridine group with sulfonyl



**Scheme 6.** Reagents and conditions: (i) compound **1c**, DCC, HOBT, DMF, rt, 8 h; (ii) bis(pinacolato)diboron, Pd(dppf)Cl<sub>2</sub>, KOAc, dry 1,4-dioxane, 100 °C, 12 h; (iii) compound **12**, Pd(dppf)Cl<sub>2</sub>·CH<sub>2</sub>Cl<sub>2</sub>, 2 M Na<sub>2</sub>CO<sub>3</sub> aq, 1,4-dioxane, 100 °C, 3 h.



**Scheme 7.** Reagents and conditions: (i) NaN<sub>3</sub>, (*n*-Bu)<sub>4</sub>N<sup>+</sup>Br<sup>-</sup>, DMSO, rt, overnight; (ii) 4-ethynyl-2-fluorobenzonitrile, K<sub>2</sub>CO<sub>3</sub>, CuSO<sub>4</sub>·5H<sub>2</sub>O, VcNa, *t*-BuOH-H<sub>2</sub>O (1:1), rt, 14 h; (iii) 80% NH<sub>2</sub>NH<sub>2</sub>·H<sub>2</sub>O, *n*-BuOH, 125 °C, 2 h; (iv) cyclopropane carbonyl chloride, DIEA, THF, rt, 18 h; then 2 M K<sub>2</sub>CO<sub>3</sub> aq, MeOH-THF (1:1), rt, 1 h.

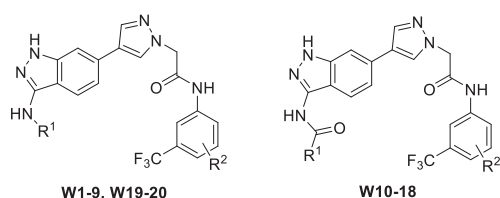
substituted phenyl, pyrazole and 2*H*-indazole ring to obtain **W2–5** with an increasing IC<sub>50</sub> values of 143–407 nM. Surprisingly, removing the substituent at the C3-amino of indazole obtained **W6** leading to IC<sub>50</sub> value increased to 12 nM. Simultaneously, the activity of **W7–9** also improved upon the replacement of R<sup>2</sup> with H, 4-Me and 2-F, and **W10–12** in which the C3-amino was acylated with cyclopropylformyl exhibited more potent anti-VEGFR-2 activity. Moreover, it could also be found that 4-Me substituted compounds **W8** and **W11** showed improved inhibitory activities with the IC<sub>50</sub> values of 2.7 nM and 1.4 nM, respectively. It illustrated that in the hinge region of VEGFR-2, the direct connection between C3-amino group and a larger sterically hindered group affected the affinity of molecule and protein, causing relatively stronger molecular rigidity. Furthermore, the suitable ClogP (2 < ClogP < 5) and ligand-lipophilic efficiency values (LLE > 4.0) [39] are used to evaluate the druggability of oral drugs for optimal physicochemical properties. **W1–5** showed an evident increase in ClogP values due to the presence of aromatic heterocycles, resulting in low LLE values, and **W6–12** exhibited relatively good values. Therefore, we selected **W11** with the most potent VEGFR-2 activity for subsequent structural optimization.

The discovery of **W11** was mainly attributed to the maintenance of the 6-(1*H*-pyrazol-4-yl)-1*H*-indazole scaffold and the simplification of the substituent groups at 3-position of indazole extending to

the solvent exposed area of VEGFR-2. Hence, exploring the substituents of C3-amino of indazole could further improve the activity. We replaced the cyclopropylformyl group with an acetyl (**W13**), isobutyryl (**W14**) and cyclopentanoyl (**W15**), and it was found that **W13** maintained potency (IC<sub>50</sub> = 1.6 nM) with a suitable ClogP. However, **W14** and **W15** resulted in a decrease in activity about 20-fold and 11-fold compared with **W11**, respectively, while the ClogP values exceeded 5. Moreover, substitution with the hydrophilic 1-methylpiperidine-4-formyl (**W16**) did not obviously increase the kinase inhibitory activity. Compared with **W1** and **W4**, when substituted with nicotianoyl (**W17**) and 1-methyl-1*H*-pyrazole-4-formyl (**W18**), the VEGFR-2 inhibitory activity was significantly increased (IC<sub>50</sub> = 2.3 vs 892 nM, 0.73 vs 220 nM, respectively), and **W18** was the most potent derivative in this series. It could be explained that the presence of the carbonyl group changed the heteroatom ring extending to the solvent exposure area, thereby reducing the steric hindrance of hinge region binding and enhancing the kinase affinity, while having better ClogP and LLE values. When replacing C3-amino with simple alkyl groups, such as ethyl (**W19**) and cyclopropylmethyl (**W20**), the VEGFR-2 inhibitory potency was greatly reduced about 27-fold and 43-fold compared with **W11**.

To further explore the effects of 6-(1*H*-pyrazol-4-yl)-1*H*-indazole skeleton to VEGFR-2 inhibitory activity, the SAR of 1*H*-pyrazol-4-yl

**Table 1**  
The *in vitro* VEGFR-2 inhibitory activity of **W1–20**.



Compound	R <sup>1</sup>	R <sup>2</sup>	VEGFR-2 inhibition <sup>a</sup>		ClogP <sup>b</sup>	LLE <sup>c</sup>
			% at 1 μM	IC <sub>50</sub> (nM)		
<b>W1</b>		4-Cl	53.8	892	5.65	0.40
<b>W2</b>		4-Cl	77.7	143	4.90	1.94
<b>W3</b>		4-Cl	77.0	249	6.40	0.20
<b>W4</b>		4-Cl	80.6	220	5.06	1.60
<b>W5</b>		4-Cl	69.6	407	6.18	0.21
<b>W6</b>	H	4-Cl	98.7	12	4.15	3.77
<b>W7</b>	H	H	99.2	7.4	3.55	4.58
<b>W8</b>	H	4-Me	98.4	2.7	4.05	4.52
<b>W9</b>	H	2-F	99.0	22	3.18	4.48
<b>W10</b>		4-Cl	99.5	14	4.91	2.94
<b>W11</b>		4-Me	100.3	1.4	4.81	4.04
<b>W12</b>		2-F	98.9	12	3.94	3.98
<b>W13</b>	Me	4-Me	104.5	1.6	4.22	4.58
<b>W14</b>	CHMe <sub>2</sub>	4-Me	103.3	28	5.06	2.49
<b>W15</b>		4-Me	93.7	15	5.70	2.12
<b>W16</b>		4-Me	98.6	11	4.28	3.68
<b>W17</b>		4-Me	102.9	2.3	4.54	4.10
<b>W18</b>		4-Me	100.4	0.73	4.05	4.81
<b>W19</b>	CH <sub>2</sub> Me	4-Me	99.6	38	5.37	2.05
<b>W20</b>		4-Me	100.3	60	5.81	1.41
<b>Sorafenib</b>	–	–	100.0	28	5.46	2.09

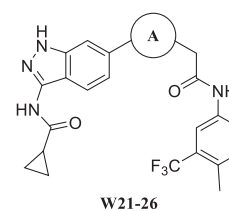
<sup>a</sup> The VEGFR-2 inhibition% at 1 μM were the average of two independent experiments.

<sup>b</sup> ClogP values were calculated using ChemDraw 14.0.

<sup>c</sup> Ligand-lipophilicity efficiency (LLE) [39] = pIC<sub>50</sub> – (ClogP).

as linker moieties was discussed and substituted with various functional group, such as 3-methyl or 3,5-dimethyl substituted 1H-pyrazol-4-yl, thiophenyl, phenyl and triazolyl (Table 2). Firstly, we introduced 3-methyl (**W21**) and 3,5-dimethyl (**W22**) to the pyrazole ring, and found that the inhibitory potency of VEGFR-2 decreased about 19-fold and 219-fold with an increasing number of methyl substitutions compared with **W11**. It was obvious that the introduction of sterically hindered substituents in the linker region affected the molecules entering the hydrophobic back pocket and

**Table 2**  
The *in vitro* VEGFR-2 inhibitory activity of **W21–26**.



Compound	A	VEGFR-2 inhibition <sup>a</sup>		ClogP <sup>b</sup>	LLE <sup>c</sup>
		% at 1 μM	IC <sub>50</sub> (nM)		
<b>W21</b>		96.2	27	4.78	2.79
<b>W22</b>		79.3	307	4.75	1.76
<b>W23</b>		98.3	12	6.14	1.78
<b>W24</b>		71.2	NT <sup>d</sup>	6.29	NT
<b>W25</b>		92.4	NT	6.29	NT
<b>W26</b>		68.5	NT	4.37	NT
<b>Sorafenib</b>	–	100.0	28	5.46	2.09

<sup>a</sup> The VEGFR-2 inhibition% at 1 μM were the average of two independent experiments.

<sup>b</sup> ClogP values were calculated using ChemDraw 14.0.

<sup>c</sup> Ligand-lipophilicity efficiency (LLE) [39] = pIC<sub>50</sub> – (ClogP).

<sup>d</sup> NT means no test.

reduced the LLE values. Secondly, about 8-fold decrease in activity was observed upon replacement of the pyrazole ring with thiophene ring (**W23**). Thirdly, distinct reduction of VEGFR-2 inhibition rate at 1 μM was found when substituted with *meta*- and *para*-substituted phenyl, and the latter **W25** was better than the former **W24**. Moreover, we synthesized a triazole compound **W26**, which displayed a decrease in VEGFR-2 activity due to its poor solubility. The above discussion illustrated that the introduction of a lipophilic thiophene, triazole or benzene ring reduced the receptor affinity and increased steric hindrance, which validated our original design strategy that the pyrazole ring of scaffold was an important part of maintaining activity and played a synergistic role with the indazole.

In summary, amidation of the 3-amino of indazole with acetyl, cyclopropylformyl, nicotianoyl and 1-methyl-1H-pyrazole-4-formyl obtained the effective VEGFR-2 inhibitors (e.g. **W8**, **W11**, **W13**, **W17** and **W18**) with IC<sub>50</sub> values lower than 3 nM. In order to further understand the mechanism of the C3-amino substituents in VEGFR-2, following molecular docking studies were carried out using Schrödinger Suite and the SAR was summarized.

### 2.3.2. Molecular docking studies

In this part, we selected **W18** with the most potent VEGFR-2 inhibition activity (IC<sub>50</sub> = 0.73 nM) as template control for docking study. As illustrated in Fig. 4A and B, the molecular docking found that **W18** inserted into the deep cleft of ATP binding site and the hydrogen atom at N<sup>1</sup> and the N<sup>2</sup> atom of indazole formed stable hydrogen bonding with Glu 917 and Cys 919 in the hinge with the distance of 2.2 Å and 2.0 Å, respectively. Besides, the terminal amide formed two key hydrogen bonding between the Glu 885 and

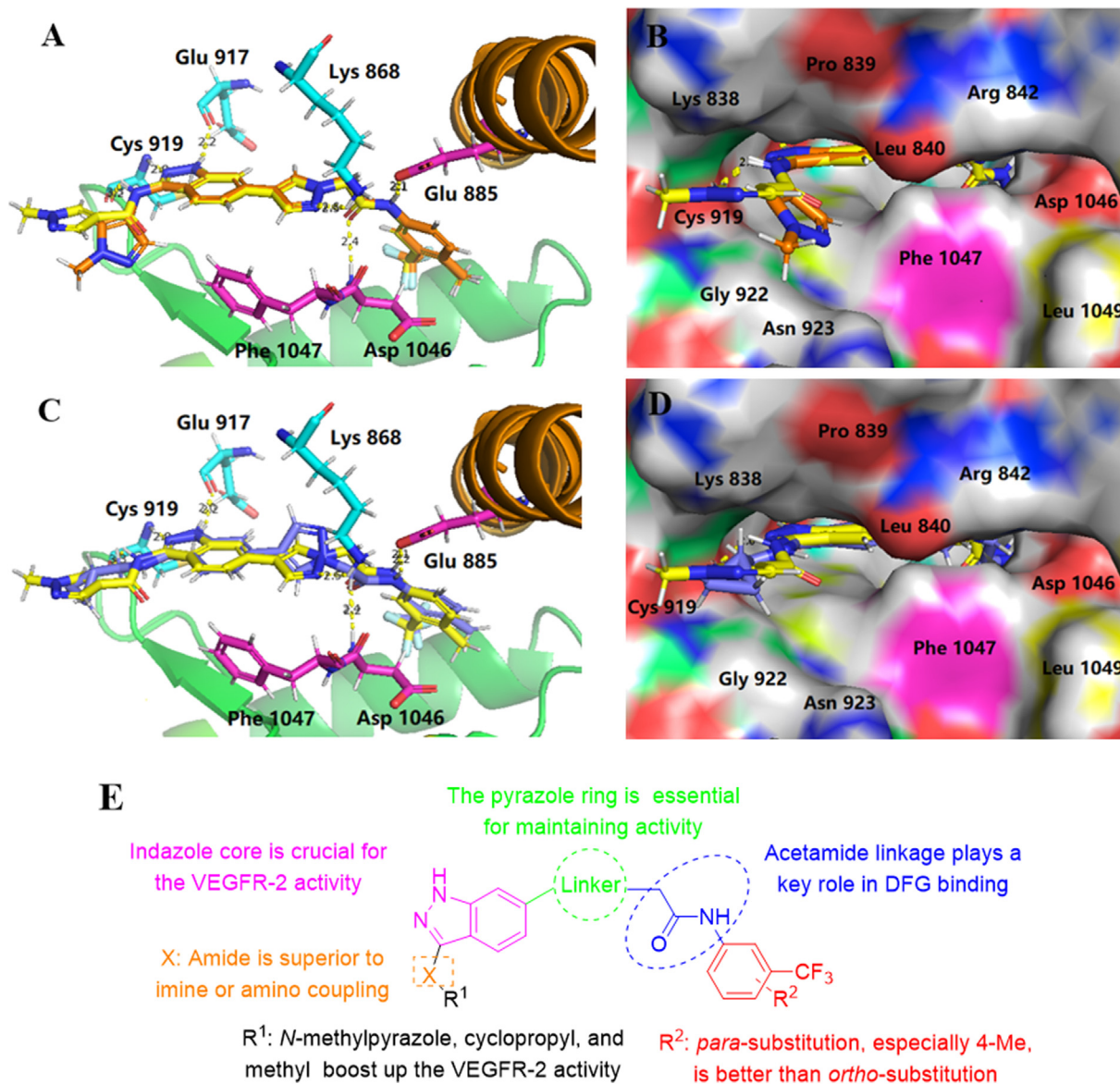


**Fig. 4.** Docking study of compounds **W4**, **W18** and **W20**. (A) Docking models of compounds **W4** (orange) and **W18** (yellow) (PDB code: 3EWH), and (B) overlap of the proposed binding mode; (C) Docking models of **W18** (yellow) and **W20** (magenta), and (D) overlap of the proposed binding modes; Yellow dashed lines indicate the hydrogen bonds and important active site residues are labeled and colored with cyan and magenta; (E) The SAR summary of synthesized target compounds.

Asp 1046 with the distance of 2.1 Å and 2.4 Å, respectively, mediating the insertion of 4-methyl-3-trifluoromethylphenyl into the hydrophobic back pocket to stabilize the DFG-out inactive conformation. Furthermore, additional hydrogen bonding was formed between the *N*<sup>2</sup> atom of pyrazole and Lys 868 with the distance of 2.5 Å, and pyrazole ring participated in a  $\pi$ - $\pi$  stacking interaction with the Phe1047 residue of VEGFR-2.

To further explore the effects of different substituents at C3-amino of indazole, docking models of compounds **W4** and **W20** were also carried out. As illustrated in Fig. 4A–4D, all compounds performed similar binding modes. The presence of 3-position amide in **W18** completely changed the direction of the pyrazole ring stretching to the solvent exposed area composed by Lys 838, Pro 839, Leu 840, Gly 841, Phe 918, Lys 920, Gly 922 and Asn 923, showing better binding conformation than amino-linked **W4**. However, the alkyl-substituted **W20** showed a poor binding mode due to its strong hydrophobic interaction with Phe 918, which

resulted in the pyrazole ring to flip and could not form a hydrogen bonding with Lys 868.

Taking *in vitro* VEGFR-2 inhibitory activities and docking results into account, the preliminary SAR as shown in Fig. 4E were obtained: (a) The 6-(1*H*-pyrazol-4-yl)-1*H*-indazol scaffold was necessary to form key hydrogen bonding interaction with Glu 917 and Cys 919, as well as the acetamide interacting with Glu 885 and Asp 1046; (b) An electron-rich five-membered ring containing nitrogen atom formed key hydrogen bonding with Lys 868; (c) 4-methyl-3-trifluoromethylphenyl was advantageous to increase the hydrophobic interaction in VEGFR-2 active site; (d) The amide structure substitution at the 3-position of indazole extended to the solvent exposure area and formed certain interaction with surrounding amino acids. These docking results provided considerable insights into the protein-ligand interactions and potential structural modifications for further drug design and activity improvement.

### 2.3.3. *In vitro* anti-proliferative evaluation

Based on the above discussion, the synthetic compounds were evaluated for their *in vitro* anti-proliferative activity using the standard MTT assay against four human cancer cells, including HT-29 (colon), A549 (lung), HepG2 (liver) and HGC-27 (gastric) [5]. Additionally, human umbilical vein endothelial cells (HUVEC) were selected as a critical *in vitro* model for antiangiogenic ability research [40], and human gastric mucosal cells (GES-1) as normal cells to evaluate the toxicity of tested compounds.

As shown in Table 3, most of the synthetic compounds exhibited comparable anti-proliferative effects in four types of tumor cells compared with the positive control sorafenib (5.13–6.18  $\mu\text{M}$ ). Moreover, the cytotoxic activity of the test compounds against gastric cancer were obviously better than those of lung cancer and liver cancer. Compounds **W5**, **W11**, **W13–16**, **W18** and **W21** manifested excellent cytotoxic activity in HGC-27 cells with  $\text{IC}_{50}$  values less than 1  $\mu\text{M}$ , especially **W18** for  $21 \pm 0.01$  nM. Furthermore, compounds **W11** and **W18** exhibited broad spectrum anti-cancer activity with all  $\text{IC}_{50}$  values below 5  $\mu\text{M}$ , and **W15** showed the most potent activity in HT-29 with  $\text{IC}_{50}$  values of  $190 \pm 0.02$  nM.

The SAR of anti-proliferation could be summarized as follows. Compounds bearing cyclopropylformyl (**W10–12**) displayed prominent growth inhibition properties on four cancer cell lines whereas C3-amino (**W6–9**) lead to a decrease of cytotoxic activity that maybe the reduced cell membrane permeability in the presence of amino group, and the inhibitory activity of 2-fluoro was weaker than 4-chloro and 4-methyl substituted. Moreover, C3-amino of indazole substituted with amide (**W13–18**) showed relatively stronger anti-cancer activity and better HUVEC cells inhibitory activity than sorafenib except **W16**. Compounds substituted with alkylamine (**W19–20**) exhibited weak inhibitory effect due to high lipophilicity. Besides, cytotoxicity could be maintained when the pyrazole ring was substituted with monomethyl (**W21**), dimethyl (**W22**) and thiophene (**W23**), while phenyl (**W24–25**) and triazole (**W26**) substitutions lost activity. Furthermore, *in vitro* GES-1 anti-proliferation evaluation showed that although majority of

the compounds performed moderate to high inhibitory activity, compounds **W13–14** and **W25–26** represented the lowest cytotoxicity with  $\text{IC}_{50}$  values more than 100  $\mu\text{M}$ . However, **W15** and **W18** exhibited obvious toxicity to normal GES-1 cells.

The results of enzyme potency and anti-proliferative activity in some compounds were inconsistent, such as **W1–5**, **W9**, **W19** and **W20**, which could be attributed to the increased ClogP values, poor physicochemical properties, cell permeability and complicated mechanism that acting on other cell signaling pathways to indirectly inhibit tumor cells survival [41,42]. Ultimately, **W13** exhibited superior VEGFR-2 inhibitory potency ( $\text{IC}_{50} = 1.6$  nM), moderate cytotoxicity on HUVEC cells ( $\text{IC}_{50} = 7.15 \pm 2.26$   $\mu\text{M}$ ), more than 500 times selectivity of tumor HGC-27 cells than normal GES-1 cells ( $\text{IC}_{50}$ :  $0.36 \pm 0.11$   $\mu\text{M}$  vs  $187.46 \pm 10.13$   $\mu\text{M}$ ), and was selected for further investigation.

### 2.3.4. Compound **W13** inhibited the colony formation of HGC-27 cells

Colony formation assay is commonly used to assess the proliferation potential and ability of adherent cells to form different colonies from a single cell [43]. In this assay, HGC-27 cells were grown in media containing different concentrations (0.1, 0.5 and 1  $\mu\text{M}$ ) of **W13** over a period of 12 days to form colonies compared with sorafenib (5  $\mu\text{M}$ ). The cells were then stained with crystal violet to visualise colonies. As shown in Fig. 5, the colony number of **W13** treated groups significantly decreased in a concentration-dependent manner, and exhibited better antiproliferation even at less concentrations than sorafenib. It was worth noting that 1  $\mu\text{M}$  of **W13** completely eliminated the colony formation, indicating strong anti-proliferation effects on HGC-27 cells.

### 2.3.5. Compound **W13** inhibited the migration and invasion of HGC-27 cells

The process of tumor cells migration, invasion and metastasis play an important role in tumor growth, which refers to individual cells separated from the primary tumor and finally entering the

**Table 3**  
The *in vitro* anti-proliferative evaluation of target compounds **W1–26** against selected cell lines.

Compound	$\text{IC}_{50}$ ( $\mu\text{M}$ ) <sup>a</sup>					
	HT-29	A549	HepG2	HGC-27	HUVEC	GES-1
<b>W1</b>	5.21 $\pm$ 0.82	7.96 $\pm$ 1.15	5.63 $\pm$ 1.00	3.65 $\pm$ 1.20	8.04 $\pm$ 0.88	12.83 $\pm$ 1.07
<b>W2</b>	3.69 $\pm$ 0.08	7.17 $\pm$ 0.70	6.54 $\pm$ 1.37	1.26 $\pm$ 0.56	7.22 $\pm$ 1.84	17.68 $\pm$ 2.94
<b>W3</b>	6.11 $\pm$ 1.12	4.72 $\pm$ 1.27	4.32 $\pm$ 1.49	5.03 $\pm$ 1.36	6.40 $\pm$ 0.59	10.02 $\pm$ 0.50
<b>W4</b>	9.17 $\pm$ 1.08	12.05 $\pm$ 0.30	10.44 $\pm$ 0.76	12.54 $\pm$ 1.78	4.03 $\pm$ 0.41	13.30 $\pm$ 2.08
<b>W5</b>	3.27 $\pm$ 0.59	1.37 $\pm$ 0.36	3.83 $\pm$ 0.29	<b>0.39 <math>\pm</math> 0.10</b>	1.45 $\pm$ 0.59	3.37 $\pm$ 0.22
<b>W6</b>	3.57 $\pm$ 1.04	12.47 $\pm$ 0.74	7.71 $\pm$ 0.32	7.68 $\pm$ 2.32	6.84 $\pm$ 1.28	11.97 $\pm$ 0.79
<b>W7</b>	3.97 $\pm$ 0.75	19.47 $\pm$ 4.67	11.53 $\pm$ 0.36	10.2 $\pm$ 0.31	7.25 $\pm$ 1.20	22.26 $\pm$ 2.02
<b>W8</b>	1.54 $\pm$ 0.15	7.09 $\pm$ 0.30	4.18 $\pm$ 0.24	4.98 $\pm$ 1.75	5.24 $\pm$ 1.52	6.96 $\pm$ 0.73
<b>W9</b>	7.83 $\pm$ 2.54	20.47 $\pm$ 2.81	13.34 $\pm$ 1.03	15.45 $\pm$ 1.19	23.85 $\pm$ 0.89	7.64 $\pm$ 0.55
<b>W10</b>	1.37 $\pm$ 0.73	8.55 $\pm$ 0.23	6.03 $\pm$ 0.003	1.05 $\pm$ 0.57	1.070 $\pm$ 0.72	29.83 $\pm$ 3.03
<b>W11</b>	<b>1.01 <math>\pm</math> 0.03</b>	<b>2.16 <math>\pm</math> 0.19</b>	<b>2.51 <math>\pm</math> 0.13</b>	<b>0.63 <math>\pm</math> 0.24</b>	<b>0.95 <math>\pm</math> 0.88</b>	4.24 $\pm$ 1.61
<b>W12</b>	5.06 $\pm$ 0.77	8.82 $\pm$ 1.52	5.61 $\pm$ 0.56	3.73 $\pm$ 0.73	5.26 $\pm$ 1.21	25.03 $\pm$ 2.73
<b>W13</b>	2.97 $\pm$ 0.90	4.31 $\pm$ 1.67	15.02 $\pm$ 2.88	<b>0.36 <math>\pm</math> 0.11</b>	7.15 $\pm$ 2.26	187.46 $\pm$ 10.13
<b>W14</b>	<b>0.48 <math>\pm</math> 0.41</b>	2.48 $\pm$ 1.41	13.66 $\pm$ 2.40	<b>0.39 <math>\pm</math> 0.11</b>	2.43 $\pm$ 0.10	>100
<b>W15</b>	<b>0.19 <math>\pm</math> 0.02</b>	1.58 $\pm$ 0.70	8.34 $\pm$ 1.31	<b>0.50 <math>\pm</math> 0.13</b>	1.49 $\pm$ 0.21	0.75 $\pm$ 0.45
<b>W16</b>	1.79 $\pm$ 0.66	5.28 $\pm$ 0.96	15.27 $\pm$ 1.22	<b>0.16 <math>\pm</math> 0.01</b>	53.88 $\pm$ 1.30	5.31 $\pm$ 1.28
<b>W17</b>	7.78 $\pm$ 1.22	5.34 $\pm$ 0.93	9.08 $\pm$ 0.63	1.17 $\pm$ 0.58	1.75 $\pm$ 0.24	8.46 $\pm$ 0.75
<b>W18</b>	<b>4.92 <math>\pm</math> 1.01</b>	<b>3.86 <math>\pm</math> 0.97</b>	<b>2.61 <math>\pm</math> 0.26</b>	<b>0.021 <math>\pm</math> 0.01</b>	4.41 $\pm$ 2.71	1.67 $\pm$ 0.84
<b>W19</b>	8.32 $\pm$ 2.86	8.48 $\pm$ 2.19	15.11 $\pm$ 2.15	1.19 $\pm$ 0.24	>50	1.90 $\pm$ 0.74
<b>W20</b>	10.96 $\pm$ 1.93	9.88 $\pm$ 1.28	22.29 $\pm$ 1.26	1.22 $\pm$ 0.12	17.94 $\pm$ 0.60	11.99 $\pm$ 1.70
<b>W21</b>	7.03 $\pm$ 0.62	1.65 $\pm$ 0.50	20.35 $\pm$ 1.97	<b>0.65 <math>\pm</math> 0.16</b>	4.92 $\pm$ 2.98	3.09 $\pm$ 1.40
<b>W22</b>	14.7 $\pm$ 0.4	1.81 $\pm$ 1.03	27.39 $\pm$ 3.37	2.79 $\pm$ 0.91	6.62 $\pm$ 0.70	11.86 $\pm$ 1.83
<b>W23</b>	8.09 $\pm$ 1.29	<b>0.96 <math>\pm</math> 0.59</b>	38.12 $\pm$ 1.24	3.09 $\pm$ 1.10	5.62 $\pm$ 1.23	13.86 $\pm$ 3.11
<b>W24</b>	>50	20.85 $\pm$ 2.16	25.51 $\pm$ 2.78	15.56 $\pm$ 3.34	>50	48.50 $\pm$ 2.92
<b>W25</b>	44.74 $\pm$ 4.24	45.14 $\pm$ 2.27	>50	33.71 $\pm$ 5.53	>100	>100
<b>W26</b>	>50	>50	>50	>50	<1	>100
<b>Sorafenib</b>	5.57 $\pm$ 0.53	5.13 $\pm$ 1.06	6.18 $\pm$ 0.36	5.22 $\pm$ 0.96	8.33 $\pm$ 3.55	9.59 $\pm$ 2.48

<sup>a</sup> Cells were treated with drugs for 72 h following MTT-based viability assay, and  $\text{IC}_{50}$  values presented as mean  $\pm$  standard error (S.E.) of three independent experiments.

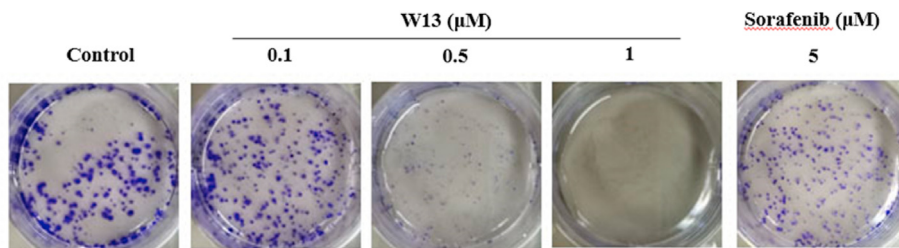


**Fig. 5.** Compound **W13** inhibited the colony formation of HGC-27 cells. HGC-27 cells were treated with indicated concentrations (0, 0.1, 0.5 and 1  $\mu\text{M}$ ) of **W13** and 5  $\mu\text{M}$  of sorafenib for 12 days, and the colonies were stained by crystal violet.

lymphatic vessels, blood or other tissues [44]. At first, a wound healing assay was performed on HGC-27 cells to investigate the inhibitory effect of **W13** on migration ability, and the results were shown in Fig. 6A. The control cells nearly migrated to fill the initial clear area after 24 h, while **W13** treatment obviously reduced HGC-27 cells migration in both dose- and time-dependent manner. Quantification of relative closure of scratches displayed that 0.5  $\mu\text{M}$  of **W13** suppressed HGC-27 migration by 9.5% and 28.0% at 6 and 24 h compared with the control (Fig. 6D).

Moreover, we further evaluated the invasion and migration ability of **W13** on HGC-27 cells by Transwell assay. As shown in Fig. 6B, it was clearly observed that **W13** reduced the penetration of HGC-27 cells through the chamber membrane under the increasing concentrations for 24 h. The number of migration cells decreased to 212, 87 and 22 from 320, respectively, compared with control group (Fig. 6E). Moreover, **W13** also induced dose-dependent suppression of the invasion of HGC-27 cells at the same concentration administration for 24 h (Fig. 6C). Quantitative statistical results indicated that **W13** significantly suppressed HGC-27 cells from invasion and reasoned its potent effect in tumor proliferation inhibition (Fig. 6F).

### 2.3.6. Compound **W13** regulated MMP-9 and E-cadherin in HGC-27 cells

MMP-9 promotes tumor cells invasion and metastasis by degrading extracellular matrix and basement membrane, regulating cell adhesion and promoting tumor cell immune escape [45]. As an effective tumor suppressor, downregulation of E-cadherin is often found in malignant epithelial cancers, which leads to metastatic dissemination and activation of EMT transcription factors [46]. As shown in Fig. 7A and B, it was clearly observed that **W13** dose-dependently decreased the MMP-9 expression and 1  $\mu\text{M}$  of **W13** significantly increased the expression level of E-cadherin protein, which could enhance cell adhesion ability and weaken cell invasiveness.

### 2.3.7. Compound **W13** induced the apoptosis of HGC-27 cells

Apoptosis involves activating, expressing and regulating a series of internal pathway proteins, and leading to programmed cell death to maintain tissue homeostasis [47]. To investigate the action mechanism of **W13** on HGC-27 cells, Annexin V-FITC/Propidium iodide (PI) dual staining assay based flow cytometry was performed. As shown in Fig. 8A, after treatment of HGC-27 with **W13** for 24 h, it was an evident enhancement of Annexin V-FITC/PI-positive apoptotic cells, in which the percentage of total apoptotic cells increased to 28.8% at 1  $\mu\text{M}$ , and higher than sorafenib with 25.4% at 5  $\mu\text{M}$ . These above results indicated that **W13** could concentration-dependently induce both early and late apoptosis in HGC-27 cells.

When tumor cells undergo apoptosis, it often disrupts the redox equilibration and causes a decrease in mitochondrial membrane potential, leading to the generation and accumulation of reactive

oxygen species (ROS) [48]. Therefore, monitoring the level of ROS in tumor cells indirectly reflect the progress and mechanism of apoptosis. In this assay, HGC-27 cells were incubated with indicated concentrations of **W13** for 24 h and stained with 2,7-dichlorodihydrofluorescein diacetate (DCFH-DA), in which the fluorescence intensity gradually increased after the drug administration using flow cytometry. As shown in Fig. 8B, **W13** could effectively increase the expression of intracellular ROS in a concentration-dependent manner compared with the control, and the fluorescence intensity increased to 945 from 712 at 0.5  $\mu\text{M}$  concentration.

Furthermore, Western blot analysis explained the mechanism that **W13** treatment dose-dependently up-regulated the expression of pro-apoptotic protein BAX and down-regulated the expression of anti-apoptotic protein Bcl-xL (Fig. 8C and D).

### 2.3.8. Compound **W13** blocked the PI3K/AKT/mTOR pathway of HGC-27 cells

Angiogenesis is the basis for the invasion and metastasis of gastric cancer cells, and the high expression of VEGF leads to the increase of micro vessel density (MVD) and abnormal proliferation of gastric cancer cells [49]. PI3K-Akt-mTOR, as one of the main downstream signaling pathways of VEGFR-2, regulates angiogenesis and vascular permeability by strengthening the survival and proliferation of endothelial cells, as well as over-activated in gastric cancer cells [50,51]. As illustrated in Fig. 9A and B, **W13** suppressed VEGFR-2 phosphorylation with a concentration dependent manner in HGC-27 cells. Effective downregulations of p-PI3K (Tyr607), p-AKT (Thr308), p-mTOR (Ser2448) and p-VEGFR-2 (Tyr1175) were observed with 0.1, 0.5 and 1  $\mu\text{M}$  of **W13** treatment. These results demonstrated that **W13** inhibited HGC-27 cells proliferation and apoptosis by downregulating the PI3K-Akt-mTOR pathway.

Taken together, our data demonstrated that compound **W13** displayed distinct antiangiogenic activity against tumor apoptosis and migration by blocking the PI3K-Akt-mTOR pathway, down-regulating Bcl-xL and MMP-9, and upregulating BAX and E-cadherin expression.

### 2.3.9. Compounds **W13** inhibited the tube formation of HUVECs

In the early stage of neovascularization, endothelial cells are recruited by neoplastic cells and polarized to form a lumen-like structure [52]. To further investigate the antiangiogenic effects of **W13**, matrigel tube formation assay of HUVECs was performed. As shown in Fig. 10A, it was clearly that integrated tubes could be found on Matrigel matrix in the control group. After adding 1, 2.5, 5 and 10  $\mu\text{M}$  of **W13** for 12 h, the HUVECs tube length, tube surface area, and the number of branch points were significantly suppressed. The results of the matrigel assay confirmed that **W13** inhibited the tube formation in a dose-dependent manner and similar effect was observed with the standard drug sorafenib. In addition, **W13** at 1, 2.5 and 5  $\mu\text{M}$  alone had no obvious cytotoxicity

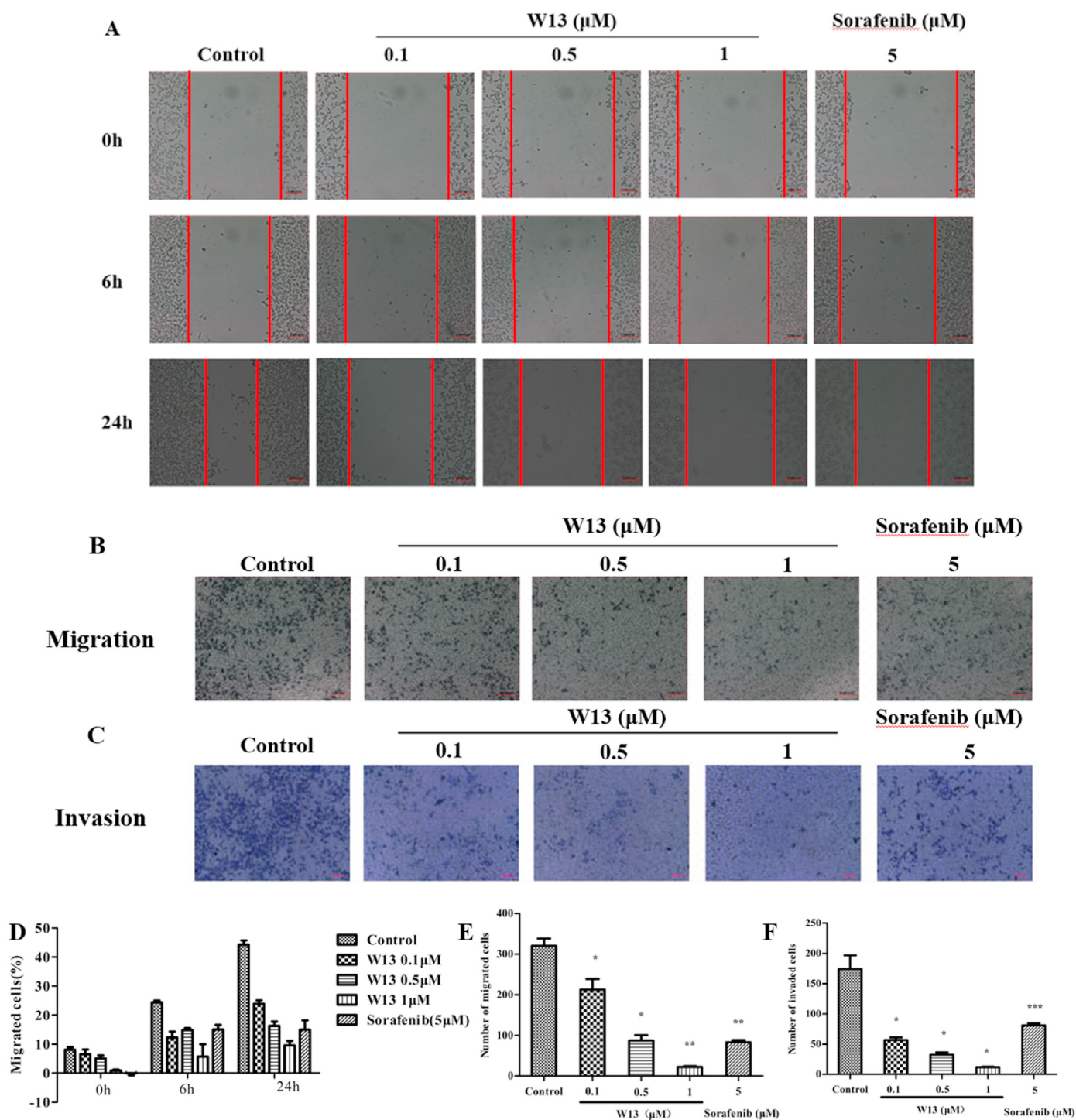


**Fig. 6.** Compound **W13** inhibited the colony formation, migration and invasion of HGC-27 cells. (A, D) HGC-27 cells were treated with indicated concentrations (0, 0.1, 0.5 and 1  $\mu\text{M}$ ) of **W13** and 1  $\mu\text{M}$  of sorafenib for 0, 6 and 24 h, and quantitative analysis of the number of relative closure of scratches in wound healing assay; (B, E) HGC-27 cells were treated with indicated concentrations of **W13** for 24 h and stained with 0.1% crystal violet solution, and quantitative analysis of the number of migrated cells in transwell migration assay; (C, F) The effect of **W13** in transwell invasion assay. All results performed above are presented as mean  $\pm$  SD from three independent experiments. \* $P < 0.05$ , \*\* $P < 0.01$ , \*\*\* $P < 0.001$  compared to the control group.

on HUVECs for 72 h in MTT assay. The results revealed that the inhibition of VEGF-induced tube formation in HUVEC cells was not due to cytotoxicity. The statistical analysis results demonstrated that compared with the control group, the tube formation ability was obviously inhibited by **W13** at low concentrations of 2.5  $\mu\text{M}$  and 5  $\mu\text{M}$  (Fig. 10B).

### 2.3.10. Compound **W13** suppressed the p-VEGFR-2 expression in HUVEC cells

It is well known that the excessive secretion of VEGF in tumor tissues usually leads to VEGF/VEGFR-2 signaling pathway over-activation during angiogenesis and rapid proliferation of endothelial cells towards tumor cells forming new capillaries. Therefore,

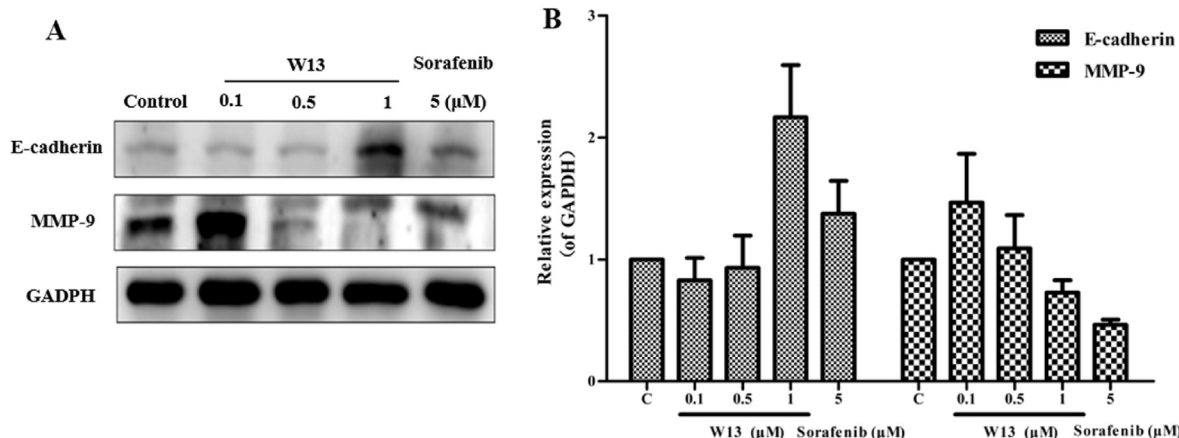


**Fig. 7.** Compound **W13** influenced the expression of MMP-9 and E-cadherin in HGC-27 cells. (A) HGC-27 cells were treated with indicated concentrations (0, 0.1, 0.5 and 1 μM) of **W13** and 1 μM of sorafenib for 24 h, and cell lysates were subjected to immunoblotting; (B) Quantitative evaluation of enzymatic activities after **W13** treatment. All results performed above are presented as mean ± SD from three independent experiments.

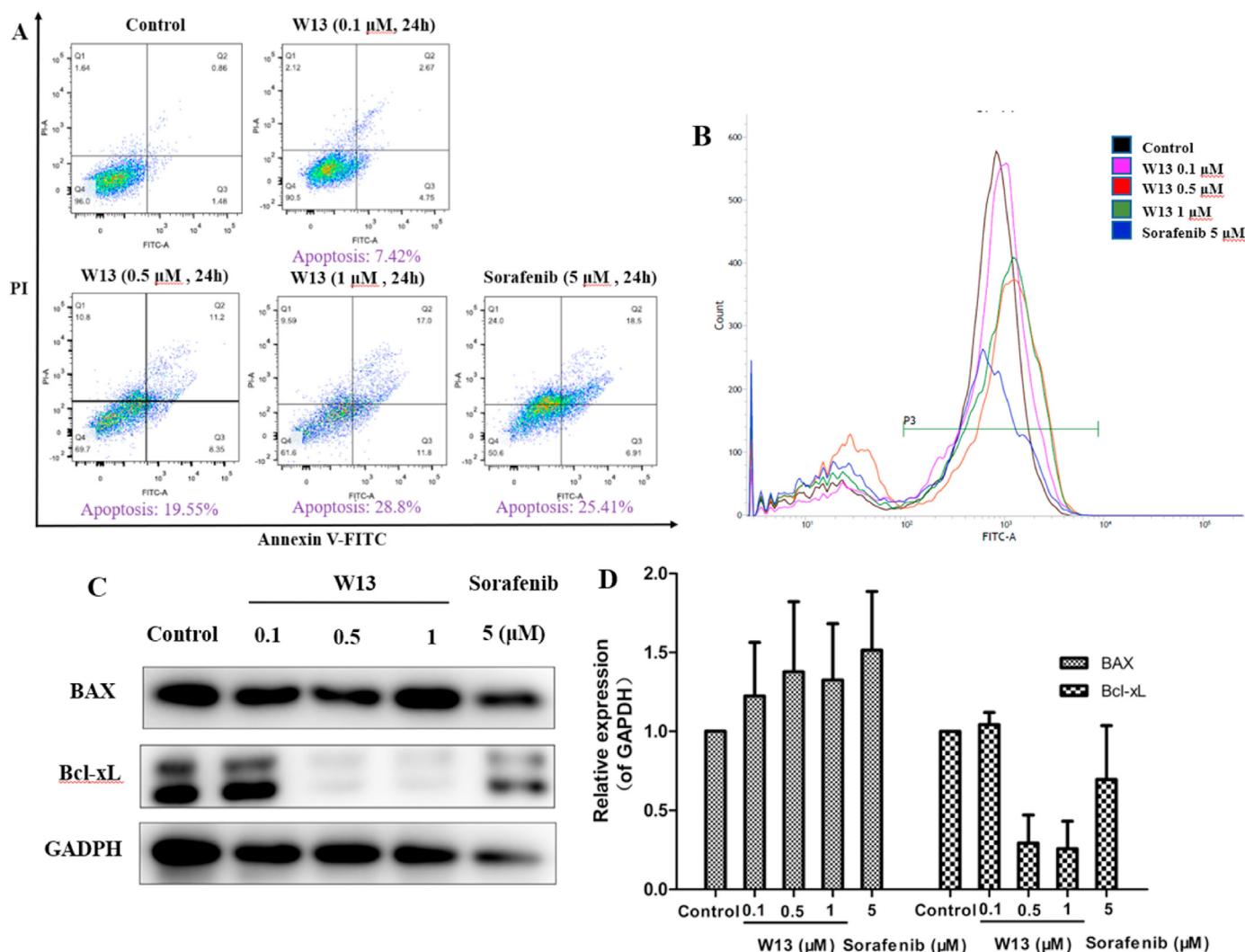


**Fig. 8.** The effect of compound **W13** on apoptosis in HGC-27 cells. (A) The quantitative analysis of HGC-27 cells treated with indicated concentrations (0, 0.1, 0.5 and 1 μM) of **W13** and 5 μM of sorafenib for 24 h, using Annexin V-FITC/PI double staining through flow cytometry. (B) HGC-27 cells were treated with the same concentrations of **W13** and sorafenib for 24 h, stained with 10 μM of DCFH-DA, and analyzed by flow cytometry; (C) Effects of **W13** and sorafenib on BAX and Bcl-xL, and cell lysates were subjected to immunoblotting; (D) Quantitative evaluation of enzymatic activities after **W13** treatment. All data were expressed as the mean ± SEM.

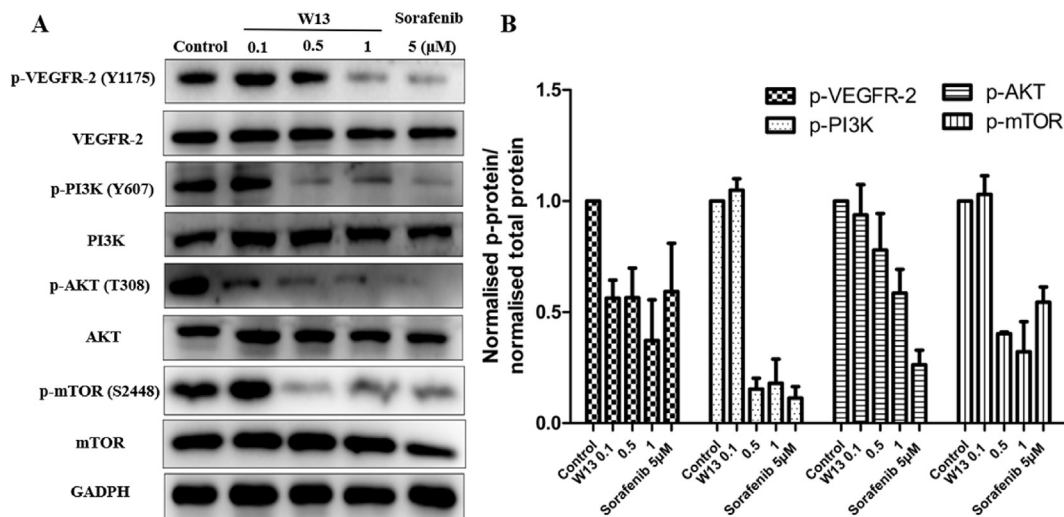


**Fig. 9.** Compound **W13** inhibited the VEGFR-2 and PI3K-Akt-mTOR signaling pathways in HGC-27 cells. (A) Effect of **W13** on both signaling pathways protein; HGC-27 cells were treated with indicated concentrations (0, 0.1, 0.5 and 1 μM) of **W13** and 5 μM of sorafenib for 24 h, and cell lysates were subjected to immunoblotting; (B) Quantitative evaluation of enzymatic activities after **W13** treatment. All data were expressed as the mean ± SEM.

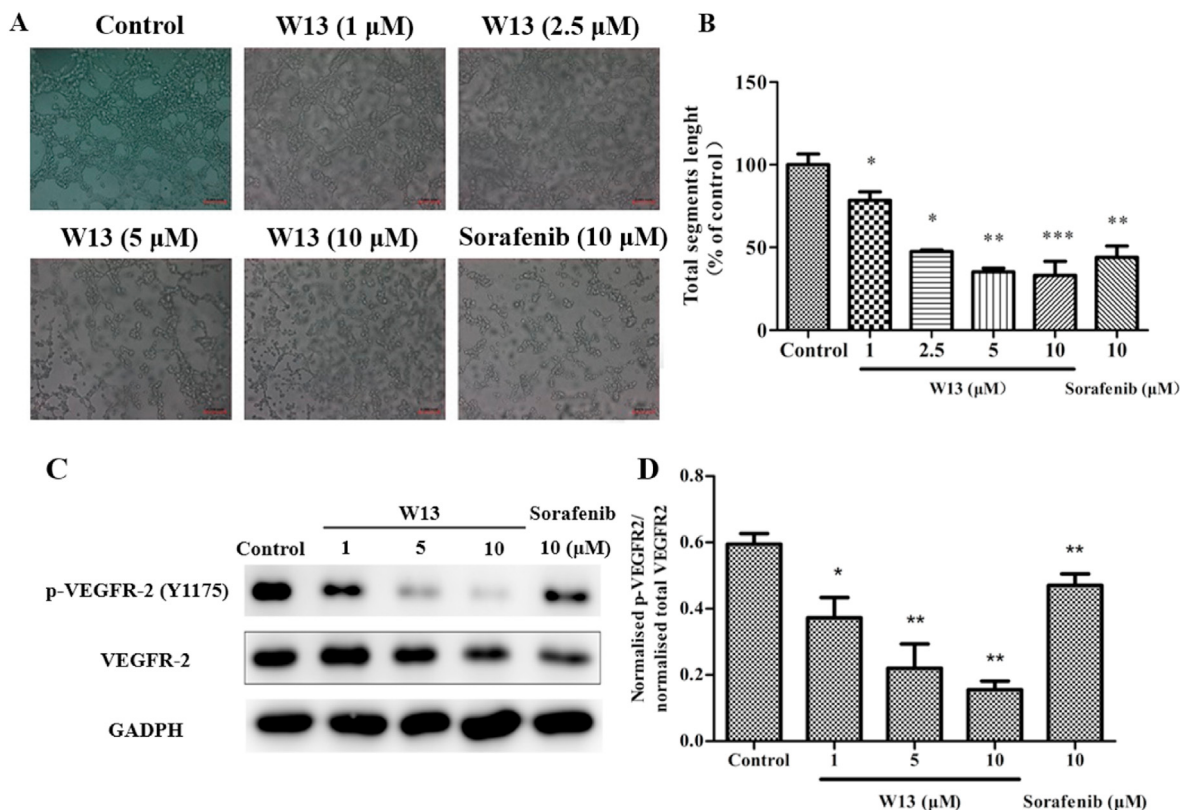


**Fig. 10.** Compound **W13** inhibited tube formation and p-VEGFR-2 expression in HUVEC cells. (A) The representative image of HUVEC cells treated with **W13** (0, 1, 2.5, 5 and 10 μM) and sorafenib (10 μM) under 20 ng/mL VEGF induction for 12 h; (B) Quantitative analysis of **W13** on tube formation in the bar graph; (C) The immunoblotting of HUVEC cells treated with indicated concentrations of **W13** and sorafenib for 24 h; (D) Quantitative evaluation of enzymatic expression after **W13** treatment. All data were expressed as the mean ± SEM. \*P < 0.05, \*\*P < 0.01, \*\*\*P < 0.001 compared to the control group.

assessing the expression of p-VEGFR-2 in VEGFR-2 overexpressed HUVEC cells using Western blot analysis can intuitively reflect the drug's inhibitory effect on angiogenesis. In this assay, HUVEC cells were seeded in 60 mm Prtri dishes (1.0 × 10<sup>6</sup> cells/dish) and incubated with increasing concentrations (0, 1, 5 and 10 μM) of **W13**

and 5 μM of sorafenib for 24 h. As illustrated in Fig. 10C and D, **W13** dose-dependently blocked the phosphorylation of VEGFR-2 compared with control group, indicating that **W13** inhibited angiogenesis by directly targeting VEGFR-2 activation in HUVEC cells.

### 3. Conclusion

Gastric cancer is one of the malignant tumors with high incidence and mortality, and it is difficult to diagnose at the early stage. In this work, a novel series of 2-(4-(1*H*-indazol-6-yl)-1*H*-pyrazol-1-yl)acetamide derivatives were designed and synthesized as VEGFR-2 inhibitors based on scaffold equivalent replacement strategy, and assessed its potential in enzymatic assay, anti-proliferation and anti-angiogenesis effect. The representative compound **W13** revealed a moderate cytotoxicity on HUVEC cells and more than 500 times selectivity of tumor HGC-27 cells than normal GES-1 cells indicating lowest toxicity. Moreover, the SAR and molecular docking studies pointed that 6-(1*H*-pyrazol-4-yl)-1*H*-indazol was essential scaffold for maintaining excellent activity.

It was found that **W13** obviously inhibited colony formation, transwell migration and invasion of HGC-27 cells in a dose-dependent manner. Further mechanism investigation revealed that **W13** could induce apoptosis by increasing ROS production and influencing apoptotic protein BAX and Bcl-xL expression in HGC-27 cells. In addition, **W13** not only blocked the PI3K-Akt-mTOR signaling pathway of HGC-27 cells, it also significantly reduced the MMP-9 expression and increased the expression of E-cadherin to prevent HGC-27 cells invasion and metastasis. Moreover, anti-angiogenesis of **W13** was evident by inhibiting tube formation and the expression of p-VEGFR-2 in HUVEC cells. All the results demonstrated that **W13** could be as a promising lead candidate for further research and structure optimization to facilitate the discovery of effective VEGFR-2 inhibitors for gastric cancer therapy.

### 4. Experimental

#### 4.1. Chemistry

##### 4.1.1. General

All reagents and solvents were used as purchased from commercial sources and used without further purified. Reactions were monitored by thin-layer chromatography (TLC) analysis (0.25 mm silica gel GF<sub>254</sub>, Yantai Xinnuo Chemical Co., Ltd., china). Column chromatography (CC) was performed on Silica Gel 60 (200–300 mesh, Yantai Xinnuo Chemical Co., Ltd., China). Melting points were determined in Kofler apparatus and were uncorrected. <sup>1</sup>H NMR and <sup>13</sup>C NMR spectra were recorded with Agilent NMR inova 600 or Bruker AM 400 spectrometers with TMS as an internal standard, all chemical shift values are reported as  $\delta$  ppm. Mass spectra were recorded on a Bruker Dalton APEXII49e and Esquire 6000 (ESI-ION TRAP) spectrometer with ESI source as ionization, respectively. The purities of all target compounds were estimated by Waters 1525 Binary HPLC Pump, and in each case, the major peak accounted for  $\geq 95\%$  of the combined total peak area when monitored by a UV detector. (The intermediate data of yield and <sup>1</sup>H NMR were provided in Supplementary Material, and only the <sup>1</sup>H NMR of the boronic ester side chain intermediates were listed here).

##### 4.1.2. General procedure for the synthesis of compounds **3a–d**

A mixture of compound **2a–d** (9.0 mmol, 1.1 eq), 4-(4,4,5,5-tetramethyl-1,3,2-dioxaborolan-2-yl)-1*H*-pyrazole (8.2 mmol, 1.0 eq), KI (1.6 mmol, 0.2 eq) and Cs<sub>2</sub>CO<sub>3</sub> (16.4 mmol, 2.0 eq) in acetonitrile was heated to reflux for 4 h under argon. The reaction was monitored by TLC and filtered through a pad of Celite, and the filtrate was concentrated in vacuo. The residue was purified by column chromatography (DCM: acetone = 100:1–5:1) to afford compounds **3a–d**.

4.1.2.1. *N*-(4-chloro-3-(trifluoromethyl)phenyl)-2-(4-(4,4,5,5-tetramethyl-1,3,2-dioxaborolan-2-yl)-1*H*-pyrazol-1-yl)acetamide

(**3a**). Yellow solid powder; yield 61%; <sup>1</sup>H NMR (600 MHz, CDCl<sub>3</sub>)  $\delta$  8.22 (s, 1 H), 7.86 (s, 1 H), 7.77 (d, *J* = 8.4 Hz, 1 H), 7.51 (d, *J* = 8.4 Hz, 1 H), 4.05 (s, 2 H).

4.1.2.2. 2-(4-(4,4,5,5-tetramethyl-1,3,2-dioxaborolan-2-yl)-1*H*-pyrazol-1-yl)-*N*-(3-(trifluoromethyl)phenyl)acetamide (**3b**). Yellow solid powder; yield 73%; <sup>1</sup>H NMR (600 MHz, CDCl<sub>3</sub>)  $\delta$  8.84 (s, 1 H), 7.99 (s, 1 H), 7.90 (s, 1 H), 7.83 (s, 1 H), 7.66 (d, *J* = 7.8 Hz, 1 H), 7.42 (d, *J* = 7.8 Hz, 1 H), 7.37 (d, *J* = 7.8 Hz, 1 H), 4.96 (s, 2 H), 1.33 (s, 12 H).

4.1.2.3. *N*-(4-methyl-3-(trifluoromethyl)phenyl)-2-(4-(4,4,5,5-tetramethyl-1,3,2-dioxaborolan-2-yl)-1*H*-pyrazol-1-yl)acetamide (**3c**). Pale yellow solid powder; yield 94%; <sup>1</sup>H NMR (600 MHz, CDCl<sub>3</sub>)  $\delta$  8.63 (s, 1 H), 7.98 (s, 1 H), 7.82 (s, 1 H), 7.63 (s, 1 H), 7.58 (d, *J* = 7.8 Hz, 1 H), 7.22 (d, *J* = 8.4 Hz, 1 H), 4.95 (s, 2 H), 2.42 (s, 3 H), 1.33 (s, 12 H).

4.1.2.4. *N*-(2-fluoro-5-(trifluoromethyl)phenyl)-2-(4-(4,4,5,5-tetramethyl-1,3,2-dioxaborolan-2-yl)-1*H*-pyrazol-1-yl)acetamide (**3d**). Reddish brown liquid; yield 34%; <sup>1</sup>H NMR (600 MHz, CDCl<sub>3</sub>)  $\delta$  9.11 (s, 1 H), 8.65 (d, *J* = 4.8 Hz, 1 H), 7.99 (s, 1 H), 7.82 (s, 1 H), 7.34 (s, 1 H), 7.18–7.15 (m, 1 H), 4.99 (s, 2 H), 1.33 (s, 12 H).

##### 4.1.3. General procedure for the synthesis of target compounds **W1–5**

To a mixture of compound **9a–e** (0.7 mmol, 1.0 eq), compound **3a** (1.3 eq) and Pd(dppf)Cl<sub>2</sub>·CH<sub>2</sub>Cl<sub>2</sub> (0.1 eq) in 1,4-dioxane (4.0 mL) was added 2 M Na<sub>2</sub>CO<sub>3</sub> aq (0.4 mL) and purged with argon. The resulting mixture was refluxed for 3 h. The reaction mixture was filtered and filtrate was evaporated in vacuo, the crude product was further purified by silica gel flash chromatography (DCM: MeOH = 100:1–20:1) to obtain target compounds **W1–5**.

4.1.3.1. *N*-(4-chloro-3-(trifluoromethyl)phenyl)-2-(4-(3-(pyridin-3-ylamino)-1*H*-indazol-6-yl)-1*H*-pyrazol-1-yl)acetamide (**W1**). Pale yellow solid powder; yield 37%; m.p.: 205–206 °C; <sup>1</sup>H NMR (600 MHz, DMSO-*d*<sub>6</sub>)  $\delta$  12.10 (s, 1 H), 10.85 (s, 1 H), 9.13 (s, 1 H), 8.85 (s, 1 H), 8.32 (s, 1 H), 8.21 (s, 1 H), 8.18 (d, *J* = 7.8 Hz, 1 H), 8.04 (s, 2 H), 7.96 (d, *J* = 8.4 Hz, 1 H), 7.85 (d, *J* = 8.4 Hz, 1 H), 7.72 (d, *J* = 9.0 Hz, 1 H), 7.55 (s, 1 H), 7.35 (d, *J* = 7.8 Hz, 1 H), 7.29 (s, 1 H), 5.11 (s, 2 H); <sup>13</sup>C NMR (150 MHz, DMSO-*d*<sub>6</sub>)  $\delta$  166.2, 144.4, 141.3, 139.6, 138.0, 137.1, 132.3, 131.2, 129.3, 124.3, 124.0, 123.5, 122.4, 121.7, 120.3, 117.9, 117.2, 112.9, 104.9, 54.7. MS (ESI) *m/z* 512.2 for [M+H]<sup>+</sup>. HRMS (ESI) *m/z* calculated for C<sub>24</sub>H<sub>18</sub>ClF<sub>3</sub>N<sub>7</sub>O [M+H]<sup>+</sup> 512.1213, found 512.1200. HPLC purity 96.4% (MeOH: H<sub>2</sub>O = 80 : 20, 0.8 mL/min, t<sub>R</sub> = 5.69 min).

4.1.3.2. *N*-(4-chloro-3-(trifluoromethyl)phenyl)-2-(4-(3-((methylsulfonyl)methyl)phenylamino)-1*H*-indazol-6-yl)-1*H*-pyrazol-1-yl)acetamide (**W2**). Pale yellow solid powder; yield 47%; m.p.: 226–228 °C; <sup>1</sup>H NMR (600 MHz, DMSO-*d*<sub>6</sub>)  $\delta$  12.00 (s, 1 H), 10.83 (s, 1 H), 8.98 (s, 1 H), 8.30 (s, 1 H), 8.21 (s, 1 H), 8.02 (s, 1 H), 7.96 (d, *J* = 8.4 Hz, 1 H), 7.85 (d, *J* = 8.4 Hz, 1 H), 7.75 (d, *J* = 7.2 Hz, 1 H), 7.72 (d, *J* = 8.4 Hz, 1 H), 7.67 (s, 1 H), 7.53 (s, 1 H), 7.32–7.27 (m, 2 H), 6.86 (d, *J* = 7.2 Hz, 1 H), 5.10 (s, 2 H), 4.43 (s, 2 H), 2.95 (s, 3 H); <sup>13</sup>C NMR (150 MHz, DMSO-*d*<sub>6</sub>)  $\delta$  166.1, 144.7, 143.5, 143.3, 141.3, 138.0, 137.1, 132.2, 131.0, 129.2, 129.1, 128.8, 126.7, 126.5, 124.3, 124.0, 123.6, 122.5, 121.3, 120.5, 118.0, 117.0, 115.7, 113.1, 104.8, 60.0, 54.7. MS (ESI) *m/z* 603.1 for [M+H]<sup>+</sup>. HRMS (ESI) *m/z* calculated for C<sub>27</sub>H<sub>23</sub>ClF<sub>3</sub>N<sub>6</sub>O<sub>3</sub>S [M+H]<sup>+</sup> 603.1193, found 603.1174. HPLC purity 96.5% (MeOH: H<sub>2</sub>O = 80 : 20, 0.8 mL/min, t<sub>R</sub> = 5.12 min).

4.1.3.3. *N*-(4-chloro-3-(trifluoromethyl)phenyl)-2-(4-(3-((2-methyl-2*H*-indazol-6-yl)amino)-1*H*-indazol-6-yl)-1*H*-pyrazol-1-yl)acetamide (**W3**). Pale yellow solid powder; yield 48%; m.p.:

162–164 °C; <sup>1</sup>H NMR (600 MHz, DMSO-*d*<sub>6</sub>) δ 12.02 (s, 1 H), 10.85 (s, 1 H), 8.85 (s, 1 H), 8.31 (s, 1 H), 8.22 (d, *J* = 1.8 Hz, 1 H), 8.17 (s, 1 H), 8.13 (s, 1 H), 8.03 (s, 1 H), 8.00 (d, *J* = 9.0 Hz, 1 H), 7.86–7.84 (m, 1 H), 7.72 (d, *J* = 8.4 Hz, 1 H), 7.55–7.54 (m, 2 H), 7.32 (d, *J* = 9.0 Hz, 1 H), 7.14 (d, *J* = 7.8 Hz, 1 H), 5.11 (s, 2 H), 4.08 (s, 3 H); <sup>13</sup>C NMR (150 MHz, DMSO-*d*<sub>6</sub>) δ 166.1, 149.6, 145.1, 141.2, 140.1, 138.0, 137.1, 132.3, 131.0, 129.2, 126.9, 124.3, 124.0, 123.5, 122.5, 121.9, 120.5, 120.0, 117.8, 116.8, 116.5, 116.0, 113.2, 104.8, 98.1, 54.7. MS (ESI) *m/z* 565.2 for [M+H]<sup>+</sup>. HRMS (ESI) *m/z* calculated for C<sub>27</sub>H<sub>21</sub>ClF<sub>3</sub>N<sub>8</sub>O [M+H]<sup>+</sup> 565.1479, found 565.1462. HPLC purity 96.9% (MeOH: H<sub>2</sub>O = 80 : 20, 0.8 mL/min, t<sub>R</sub> = 5.35 min).

4.1.3.4. *N*-(4-chloro-3-(trifluoromethyl)phenyl)-2-(4-(3-((1-methyl-1H-pyrazol-4-yl) amino)-1H-indazol-6-yl)-1H-pyrazol-1-yl)acetamide (**W4**). Green solid powder; yield 31%; m.p.: 155–157 °C; <sup>1</sup>H NMR (600 MHz, DMSO-*d*<sub>6</sub>) δ 11.65 (s, 1 H), 10.83 (s, 1 H), 8.25 (s, 1 H), 8.19 (d, *J* = 3.0 Hz, 1 H), 7.97 (s, 1 H), 7.85 (s, 1 H), 7.83–7.79 (m, 3 H), 7.69 (d, *J* = 9.0 Hz, 1 H), 7.43–7.41 (m, 2 H), 7.23 (d, *J* = 7.8 Hz, 1 H), 5.07 (s, 2 H), 3.79 (s, 3 H); <sup>13</sup>C NMR (150 MHz, DMSO-*d*<sub>6</sub>) δ 166.2, 147.1, 145.9, 142.0, 138.0, 137.0, 132.3, 130.9, 129.1, 128.3, 126.2, 124.2, 124.0, 122.6, 120.2, 118.6, 117.9, 116.4, 112.1, 104.7, 79.1, 54.7. MS (ESI) *m/z* 515.2 for [M+H]<sup>+</sup>. HRMS (ESI) *m/z* calculated for C<sub>23</sub>H<sub>19</sub>ClF<sub>3</sub>N<sub>8</sub>O [M+H]<sup>+</sup> 515.1322, found 515.1307. HPLC purity 96.1% (MeOH: H<sub>2</sub>O = 80 : 20, 0.8 mL/min, t<sub>R</sub> = 5.15 min).

4.1.3.5. *N*-(4-chloro-3-(trifluoromethyl)phenyl)-2-(4-(3-(4-methyl-3-(*N*-methylsulfo moyl)phenyl)amino)-1H-indazol-6-yl)-1H-pyrazol-1-yl)acetamide (**W5**). White solid powder; yield 53%; m.p.: 210–212 °C; <sup>1</sup>H NMR (600 MHz, DMSO-*d*<sub>6</sub>) δ 12.04 (s, 1 H), 10.82 (s, 1 H), 9.15 (s, 1 H), 8.28 (s, 1 H), 8.19 (s, 2 H), 8.00 (s, 1 H), 7.93 (d, *J* = 8.4 Hz, 1 H), 7.87–7.86 (m, 1 H), 7.82 (dd, *J* = 8.4 Hz, 1.8 Hz, 1 H), 7.70 (d, *J* = 9.6 Hz, 1 H), 7.51 (s, 1 H), 7.32–7.29 (m, 2 H), 7.27 (d, *J* = 7.8 Hz, 1 H), 5.08 (s, 2 H), 2.45 (s, 3 H), 2.43 (d, *J* = 4.8 Hz, 3 H); <sup>13</sup>C NMR (150 MHz, DMSO-*d*<sub>6</sub>) δ 166.1, 144.6, 141.3, 141.0, 138.0, 137.4, 137.1, 133.0, 132.8, 132.2, 131.1, 129.2, 126.7, 125.4, 124.3, 124.0, 122.5, 120.3, 118.9, 117.8, 117.1, 116.3, 112.9, 104.8, 54.7, 28.3, 18.9. MS (ESI) *m/z* 618.1 for [M+H]<sup>+</sup>. HRMS (ESI) *m/z* calculated for C<sub>27</sub>H<sub>24</sub>ClF<sub>3</sub>N<sub>7</sub>O<sub>3</sub>S [M+H]<sup>+</sup> 618.1302, found 618.1284. HPLC purity 97.6% (MeOH: H<sub>2</sub>O = 80 : 20, 0.8 mL/min, t<sub>R</sub> = 5.46 min).

#### 4.1.4. General procedure for the synthesis of target compounds **W6**–**12**

To a mixture of compound **11** or **12** (1.0 mmol, 1.0 eq), compounds **3a**–**3d** (1.3 eq) and Pd(dppf)Cl<sub>2</sub>·CH<sub>2</sub>Cl<sub>2</sub> (0.1 eq) in 1,4-dioxane (4.0 mL) was added 2 M Na<sub>2</sub>CO<sub>3</sub> aq (0.4 mL) and purged with argon. The resulting mixture was refluxed for 3 h before being cooled to the room temperature. The reaction mixture was filtered and filtrate was evaporated in vacuo, the crude product was further purified by silica gel flash chromatography (DCM: MeOH = 100:1–20:1) to obtain target compounds **W6**–**12**.

4.1.4.1. 2-(4-(3-amino-1H-indazol-6-yl)-1H-pyrazol-1-yl)-*N*-(4-chloro-3-(trifluoro methyl)phenyl)acetamide (**W6**). Gray solid powder; yield 46%; m.p.: 226–228 °C; <sup>1</sup>H NMR (600 MHz, DMSO-*d*<sub>6</sub>) δ 11.37 (s, 1 H), 10.84 (s, 1 H), 8.25 (s, 1 H), 8.21 (s, 1 H), 7.97 (s, 1 H), 7.84 (d, *J* = 8.4 Hz, 1 H), 7.72 (d, *J* = 8.4 Hz, 1 H), 7.68 (d, *J* = 9.0 Hz, 1 H), 7.39 (s, 1 H), 7.18 (d, *J* = 8.4 Hz, 1 H), 5.42 (s, 2 H), 5.09 (s, 2 H); <sup>13</sup>C NMR (150 MHz, DMSO-*d*<sub>6</sub>) δ 166.0, 137.9, 136.9, 132.1, 130.5, 128.9, 126.8, 126.6, 124.2, 123.9, 123.4, 122.6, 121.6, 117.8, 115.9, 104.8, 54.5. MS (ESI) *m/z* 435.1 for [M+H]<sup>+</sup>. HRMS (ESI) *m/z* calculated for C<sub>19</sub>H<sub>15</sub>ClF<sub>3</sub>N<sub>6</sub>O [M+H]<sup>+</sup> 435.0948, found 435.0934. HPLC purity 95.6% (MeOH: H<sub>2</sub>O = 80 : 20, 0.8 mL/min, t<sub>R</sub> = 4.87 min).

4.1.4.2. 2-(4-(3-amino-1H-indazol-6-yl)-1H-pyrazol-1-yl)-*N*-(3-(trifluoromethyl)phenyl)acetamide (**W7**). Pale yellow solid powder;

yield 30%; m.p.: 243–245 °C; <sup>1</sup>H NMR (600 MHz, DMSO-*d*<sub>6</sub>) δ 11.30 (s, 1 H), 10.68 (s, 1 H), 8.23 (s, 1 H), 8.10 (s, 1 H), 7.95 (s, 1 H), 7.79 (d, *J* = 7.8 Hz, 1 H), 7.67 (d, *J* = 8.4 Hz, 1 H), 7.59 (d, *J* = 8.4 Hz, 1 H), 7.45 (d, *J* = 7.8 Hz, 1 H), 7.38 (s, 1 H), 7.17 (d, *J* = 8.4 Hz, 1 H), 5.27 (s, 2 H), 5.08 (s, 2 H); <sup>13</sup>C NMR (150 MHz, DMSO-*d*<sub>6</sub>) δ 166.0, 149.1, 142.2, 139.3, 136.9, 130.4, 130.1, 129.6, 129.4, 128.9, 124.9, 122.7, 120.6, 120.0, 116.0, 115.3, 112.7, 104.7, 54.7. MS (ESI) *m/z* 401.2 for [M+H]<sup>+</sup>. HRMS (ESI) *m/z* calculated for C<sub>19</sub>H<sub>16</sub>F<sub>3</sub>N<sub>6</sub>O [M+H]<sup>+</sup> 401.1338, found 401.1323. HPLC purity 98.3% (MeOH: H<sub>2</sub>O = 80 : 20, 0.8 mL/min, t<sub>R</sub> = 4.39 min).

4.1.4.3. 2-(4-(3-amino-1H-indazol-6-yl)-1H-pyrazol-1-yl)-*N*-(4-methyl-3-(trifluoro methyl)phenyl)acetamide (**W8**). Pale yellow solid powder; yield 30%; m.p.: 232–233 °C; <sup>1</sup>H NMR (600 MHz, DMSO-*d*<sub>6</sub>) δ 11.33 (s, 1 H), 10.60 (s, 1 H), 8.23 (s, 1 H), 8.03 (s, 1 H), 7.95 (s, 1 H), 7.71 (d, *J* = 7.8 Hz, 1 H), 7.67 (d, *J* = 8.4 Hz, 1 H), 7.42 (d, *J* = 7.8 Hz, 1 H), 7.38 (s, 1 H), 7.17 (d, *J* = 9.0 Hz, 1 H), 5.30 (s, 2 H), 5.06 (s, 2 H), 2.39 (s, 3 H); <sup>13</sup>C NMR (150 MHz, DMSO-*d*<sub>6</sub>) δ 165.7, 149.1, 142.2, 136.9, 136.7, 132.8, 130.7, 130.4, 128.9, 125.2, 123.4, 122.7, 122.6, 120.6, 116.2, 116.0, 112.7, 104.7, 54.6, 18.1. MS (ESI) *m/z* 415.2 for [M+H]<sup>+</sup>. HRMS (ESI) *m/z* calculated for C<sub>20</sub>H<sub>18</sub>F<sub>3</sub>N<sub>6</sub>O [M+H]<sup>+</sup> 415.1494, found 415.1480. HPLC purity 97.6% (MeOH: H<sub>2</sub>O = 80 : 20, 0.8 mL/min, t<sub>R</sub> = 4.70 min).

4.1.4.4. 2-(4-(3-amino-1H-indazol-6-yl)-1H-pyrazol-1-yl)-*N*-(2-fluoro-5-(trifluoro methyl)phenyl)acetamide (**W9**). Pale yellow solid powder; yield 20%; m.p.: 223–225 °C; <sup>1</sup>H NMR (600 MHz, DMSO-*d*<sub>6</sub>) δ 11.33 (s, 1 H), 10.51 (s, 1 H), 8.46 (d, *J* = 6.6 Hz, 1 H), 8.24 (s, 1 H), 7.97 (s, 1 H), 7.67 (d, *J* = 9.0 Hz, 1 H), 7.58–7.56 (m, 2 H), 7.38 (s, 1 H), 7.16 (d, *J* = 8.4 Hz, 1 H), 5.30 (s, 2 H), 5.19 (s, 2 H); <sup>13</sup>C NMR (150 MHz, DMSO-*d*<sub>6</sub>) δ 166.7, 155.6, 149.1, 142.2, 136.9, 130.3, 129.0, 126.8, 126.7, 122.8, 122.3, 120.6, 119.8, 116.8, 116.7, 116.0, 112.7, 104.7, 54.4. MS (ESI) *m/z* 419.1 for [M+H]<sup>+</sup>. HRMS (ESI) *m/z* calculated for C<sub>19</sub>H<sub>15</sub>F<sub>4</sub>N<sub>6</sub>O [M+H]<sup>+</sup> 419.1243, found 419.1230. HPLC purity 98.3% (MeOH: H<sub>2</sub>O = 80 : 20, 0.8 mL/min, t<sub>R</sub> = 4.35 min).

4.1.4.5. *N*-(6-(1-(2-((4-chloro-3-(trifluoromethyl)phenyl)amino)-2-oxoethyl)-1H-pyrazol-4-yl)-1H-indazol-3-yl)cyclopropanecarboxamide (**W10**). Gray solid powder; yield 31%; m.p.: 267–269 °C; <sup>1</sup>H NMR (600 MHz, DMSO-*d*<sub>6</sub>) δ 12.54 (s, 1 H), 10.79 (s, 1 H), 10.60 (s, 1 H), 8.28 (s, 1 H), 8.20 (s, 1 H), 8.00 (s, 1 H), 7.85 (d, *J* = 8.4 Hz, 1 H), 7.78 (d, *J* = 8.4 Hz, 1 H), 7.71 (d, *J* = 8.4 Hz, 1 H), 7.56 (s, 1 H), 7.29 (d, *J* = 8.4 Hz, 1 H), 5.09 (s, 2 H), 1.94 (s, 1 H), 0.85–0.83 (m, 4 H); <sup>13</sup>C NMR (150 MHz, DMSO-*d*<sub>6</sub>) δ 171.6, 166.1, 141.8, 140.5, 138.0, 137.0, 132.2, 130.6, 129.2, 126.7, 124.3, 124.0, 123.0, 122.3, 121.7, 117.9, 114.7, 113.1, 105.0, 54.7, 13.6, 7.1. MS (ESI) *m/z* 503.1 for [M+H]<sup>+</sup>. HRMS (ESI) *m/z* calculated for C<sub>23</sub>H<sub>19</sub>ClF<sub>3</sub>N<sub>6</sub>O<sub>2</sub> [M+H]<sup>+</sup> 503.1210, found 503.1195. HPLC purity 97.8% (MeOH: H<sub>2</sub>O = 80 : 20, 0.8 mL/min, t<sub>R</sub> = 5.32 min).

4.1.4.6. *N*-(6-(1-(2-((4-methyl-3-(trifluoromethyl)phenyl)amino)-2-oxoethyl)-1H-pyrazol-4-yl)-1H-indazol-3-yl)cyclopropanecarboxamide (**W11**). Pale yellow solid powder; yield 46%; m.p.: 247–249 °C; <sup>1</sup>H NMR (600 MHz, DMSO-*d*<sub>6</sub>) δ 12.57 (s, 1 H), 10.64 (s, 1 H), 10.61 (s, 1 H), 8.29 (s, 1 H), 8.03 (d, *J* = 1.8 Hz, 1 H), 8.01 (s, 1 H), 7.78 (d, *J* = 9.0 Hz, 1 H), 7.71 (d, *J* = 9.0 Hz, 1 H), 7.56 (s, 1 H), 7.42 (d, *J* = 7.8 Hz, 1 H), 7.29 (d, *J* = 8.4 Hz, 1 H), 5.07 (s, 2 H), 2.39 (s, 3 H), 1.94 (s, 1 H), 0.86–0.82 (m, 4 H); <sup>13</sup>C NMR (150 MHz, DMSO-*d*<sub>6</sub>) δ 171.6, 165.7, 141.8, 140.5, 136.9, 136.7, 132.8, 130.7, 129.2, 127.4, 125.2, 123.0, 122.5, 122.3, 117.9, 116.2, 114.7, 105.0, 54.7, 18.1, 13.6, 7.1. MS (ESI) *m/z* 483.3 for [M+H]<sup>+</sup>. HRMS (ESI) *m/z* calculated for C<sub>24</sub>H<sub>22</sub>F<sub>3</sub>N<sub>6</sub>O<sub>2</sub> [M+H]<sup>+</sup> 483.1756, found 483.1740. HPLC purity 97.5% (MeOH: H<sub>2</sub>O = 80 : 20, 1.0 mL/min, t<sub>R</sub> = 6.07 min).

4.1.4.7. *N*-(6-(1-(2-((2-fluoro-5-(trifluoromethyl)phenyl)amino)-2-oxoethyl)-1H-pyrazol-4-yl)-1H-indazol-3-yl)cyclopropanecarboxamide (**W12**). Gray solid powder; yield 35%; m.p.: 258–260 °C; <sup>1</sup>H NMR (600 MHz, DMSO-*d*<sub>6</sub>) δ 12.56 (s, 1 H), 10.63 (s, 1 H), 10.51 (s, 1 H), 8.45 (d, *J* = 6.6 Hz, 1 H), 8.29 (s, 1 H), 8.01 (s, 1 H), 7.78 (d, *J* = 9.0 Hz, 1 H), 7.58–7.56 (m, 3 H), 7.29 (d, *J* = 9.0 Hz, 1 H), 5.20 (s, 2 H), 1.94 (s, 1 H), 0.85–0.82 (m, 4 H); <sup>13</sup>C NMR (150 MHz, DMSO-*d*<sub>6</sub>) δ 171.7, 166.1, 155.6, 141.8, 140.5, 137.1, 132.2, 130.7, 129.3, 126.9, 124.6, 123.2, 122.8, 122.4, 119.8, 117.9, 116.7, 114.7, 105.0, 54.4, 13.6, 7.2. MS (ESI) *m/z* 487.2 for [M+H]<sup>+</sup>. HRMS (ESI) *m/z* calculated for C<sub>23</sub>H<sub>19</sub>F<sub>4</sub>N<sub>6</sub>O<sub>2</sub> [M+H]<sup>+</sup> 487.1506, found 487.1491. HPLC purity 97.6% (MeOH: H<sub>2</sub>O = 80 : 20, 0.8 mL/min, t<sub>R</sub> = 4.63 min).

#### 4.1.5. General procedure for the synthesis of target compounds **W13–14**

To a suspension of compound **W8** (0.4 mmol, 1.0 eq) in tetrahydrofuran (4 mL) was added acetyl chloride or isobutyryl chloride (2.4 eq) followed by DIEA (4.8 eq). After the mixture was stirred for 18 h at room temperature, it was poured into water and extracted with ethyl acetate. The combined organic layer was dried over anhydrous Na<sub>2</sub>SO<sub>4</sub> and evaporated the solvent. The residue was dissolved in tetrahydrofuran/methanol (2 mL/2 mL) and 2 N K<sub>2</sub>CO<sub>3</sub> aq (0.25 mL) was added. After stirring for 1 h, appropriate water was added and extracted with ethyl acetate. The combined organic layer was dried over anhydrous Na<sub>2</sub>SO<sub>4</sub>, concentrated, and purified by column chromatography (DCM: MeOH = 100:1–10:1) to obtain compounds **W13–14**.

4.1.5.1. 2-(4-(3-acetamido-1H-indazol-6-yl)-1H-pyrazol-1-yl)-*N*-(4-methyl-3-(trifluoromethyl)phenyl)acetamide (**W13**). White solid powder; yield 46%; m.p.: 263–265 °C; <sup>1</sup>H NMR (600 MHz, DMSO-*d*<sub>6</sub>) δ 12.61 (s, 1 H), 10.61 (s, 1 H), 10.35 (s, 1 H), 8.30 (s, 1 H), 8.03 (s, 1 H), 8.01 (s, 1 H), 7.79 (d, *J* = 8.4 Hz, 1 H), 7.71 (d, *J* = 10.8 Hz, 1 H), 7.56 (s, 1 H), 7.42 (d, *J* = 7.8 Hz, 1 H), 7.31 (d, *J* = 8.4 Hz, 1 H), 5.07 (s, 2 H), 2.39 (s, 3 H), 2.11 (s, 1 H); <sup>13</sup>C NMR (150 MHz, DMSO-*d*<sub>6</sub>) δ 168.7, 166.2, 142.3, 140.9, 137.5, 137.3, 133.3, 131.2, 129.7, 127.9, 125.7, 123.9, 123.5, 123.1, 122.8, 118.5, 116.7, 115.2, 105.5, 55.2, 23.4, 18.6. MS (ESI) *m/z* 457.3 for [M+H]<sup>+</sup>. HRMS (ESI) *m/z* calculated for C<sub>22</sub>H<sub>20</sub>F<sub>3</sub>N<sub>6</sub>O<sub>2</sub> [M+H]<sup>+</sup> 457.1600, found 457.1585. HPLC purity >99% (MeOH: H<sub>2</sub>O = 80 : 20, 1.0 mL/min, t<sub>R</sub> = 3.75 min).

4.1.5.2. *N*-(6-(1-(2-((4-methyl-3-(trifluoromethyl)phenyl)amino)-2-oxoethyl)-1H-pyrazol-4-yl)-1H-indazol-3-yl)isobutyramide (**W14**). White solid powder; yield 59%; m.p.: 219–221 °C; <sup>1</sup>H NMR (600 MHz, DMSO-*d*<sub>6</sub>) δ 12.57 (s, 1 H), 10.61 (s, 1 H), 10.25 (s, 1 H), 8.29 (s, 1 H), 8.03 (s, 1 H), 8.01 (s, 1 H), 7.75 (d, *J* = 8.4 Hz, 1 H), 7.71 (d, *J* = 6.0 Hz, 1 H), 7.57 (s, 1 H), 7.42 (d, *J* = 8.4 Hz, 1 H), 7.31 (d, *J* = 8.4 Hz, 1 H), 5.07 (s, 2 H), 2.74–2.72 (m, 1 H), 2.39 (s, 3 H), 1.17–1.15 (m, 6 H); <sup>13</sup>C NMR (150 MHz, DMSO-*d*<sub>6</sub>) δ 175.8, 166.2, 142.3, 141.0, 137.5, 137.3, 133.3, 131.2, 129.7, 127.9, 126.4, 123.9, 123.4, 123.1, 122.8, 117.9, 116.7, 115.4, 106.1, 54.4, 34.4, 20.1, 18.6. MS (ESI) *m/z* 485.3 for [M+H]<sup>+</sup>. HRMS (ESI) *m/z* calculated for C<sub>24</sub>H<sub>24</sub>F<sub>3</sub>N<sub>6</sub>O<sub>2</sub> [M+H]<sup>+</sup> 485.1913, found 485.1897. HPLC purity 99.7% (MeOH: H<sub>2</sub>O = 80 : 20, 1.0 mL/min, t<sub>R</sub> = 3.73 min).

#### 4.1.6. General procedure for the synthesis of target compounds **W15–20**

To a solution of compounds **15a–d** or **17a–b** (0.8 mmol) with dichloromethane (11 mL) was slowly added trifluoroacetate (5.00 mL) dropwise under ice water bath. After 30 min, the reaction was stirred at room temperature for 3.5 h. After the reaction was completed, the solvent was evaporated and the residue was taken up in ethyl acetate and saturated Na<sub>2</sub>CO<sub>3</sub> aq, and extracted with ethyl acetate. The combined organic phase was washed with brine and dried over Na<sub>2</sub>SO<sub>4</sub>. The solvent was concentrated in vacuo and

purified by silica gel flash chromatography (DCM: MeOH = 100:1–10:1) to obtain target compounds **W15–20**.

4.1.6.1. *N*-(6-(1-(2-((4-methyl-3-(trifluoromethyl)phenyl)amino)-2-oxoethyl)-1H-pyrazol-4-yl)-1H-indazol-3-yl)cyclopentanecarboxamide (**W15**). Yellow solid powder; yield 67%; m.p.: 233–234 °C; <sup>1</sup>H NMR (600 MHz, DMSO-*d*<sub>6</sub>) δ 12.55 (s, 1 H), 10.61 (s, 1 H), 10.25 (s, 1 H), 8.29 (s, 1 H), 8.03–7.99 (m, 2 H), 7.76 (d, *J* = 8.4 Hz, 1 H), 7.71 (d, *J* = 7.8 Hz, 1 H), 7.56 (s, 1 H), 7.42 (d, *J* = 7.8 Hz, 1 H), 7.30 (s, 1 H), 5.07 (s, 2 H), 2.91–2.90 (m, 1 H), 2.39 (s, 3 H), 1.89 (s, 2 H), 1.77 (s, 2 H), 1.70 (s, 2 H), 1.59 (s, 2 H); <sup>13</sup>C NMR (150 MHz, DMSO-*d*<sub>6</sub>) δ 175.0, 166.3, 142.3, 141.0, 137.5, 137.3, 132.4, 130.8, 129.7, 127.9, 125.7, 123.9, 123.4, 123.1, 122.8, 118.4, 117.2, 115.3, 105.1, 54.7, 45.3, 30.7, 25.6, 18.6. MS (ESI) *m/z* 511.3 for [M+H]<sup>+</sup>. HRMS (ESI) *m/z* calculated for C<sub>26</sub>H<sub>26</sub>F<sub>3</sub>N<sub>6</sub>O<sub>2</sub> [M+H]<sup>+</sup> 511.2069, found 511.2056. HPLC purity 100% (MeOH: H<sub>2</sub>O = 80 : 20, 1.0 mL/min, t<sub>R</sub> = 3.87 min).

4.1.6.2. 1-Methyl-*N*-(6-(1-(2-((4-methyl-3-(trifluoromethyl)phenyl)amino)-2-oxoethyl)-1H-pyrazol-4-yl)-1H-indazol-3-yl)piperidine-4-carboxamide (**W16**). White solid powder; yield 71%; m.p.: 178–180 °C; <sup>1</sup>H NMR (600 MHz, DMSO-*d*<sub>6</sub>) δ 12.59 (s, 1 H), 10.68 (s, 1 H), 10.29 (s, 1 H), 8.29 (s, 1 H), 8.04 (s, 1 H), 8.00 (s, 1 H), 7.75 (d, *J* = 8.4 Hz, 1 H), 7.72 (d, *J* = 8.4 Hz, 1 H), 7.57 (s, 1 H), 7.42 (d, *J* = 8.4 Hz, 1 H), 7.31 (d, *J* = 8.4 Hz, 1 H), 5.08 (s, 2 H), 2.91 (s, 2 H), 2.46 (s, 1 H), 2.39 (s, 3 H), 2.26 (s, 3 H), 2.06 (s, 2 H), 1.84 (s, 2 H), 1.75–1.73 (m, 2 H); <sup>13</sup>C NMR (150 MHz, DMSO-*d*<sub>6</sub>) δ 174.2, 166.3, 142.3, 140.8, 137.5, 137.3, 133.3, 131.2, 129.7, 127.9, 125.7, 123.9, 123.3, 123.1, 122.8, 118.4, 116.7, 115.3, 105.5, 55.6, 46.4, 41.6, 37.0, 31.2, 28.8, 21.3, 18.6. MS (ESI) *m/z* 540.3 for [M+H]<sup>+</sup>. HRMS (ESI) *m/z* calculated for C<sub>27</sub>H<sub>29</sub>F<sub>3</sub>N<sub>7</sub>O<sub>2</sub> [M+H]<sup>+</sup> 540.2335, found 540.2315. HPLC purity 95.4% (MeOH: H<sub>2</sub>O = 80 : 20, 1.0 mL/min, t<sub>R</sub> = 3.89 min).

4.1.6.3. *N*-(6-(1-(2-((4-methyl-3-(trifluoromethyl)phenyl)amino)-2-oxoethyl)-1H-pyrazol-4-yl)-1H-indazol-3-yl)nicotinamide (**W17**). Yellow solid powder; yield 90%; m.p.: 142–144 °C; <sup>1</sup>H NMR (600 MHz, DMSO-*d*<sub>6</sub>) δ 12.81 (s, 1 H), 11.04 (s, 1 H), 10.65 (s, 1 H), 9.22 (s, 1 H), 8.79 (d, *J* = 4.8 Hz, 1 H), 8.42 (d, *J* = 7.8 Hz, 1 H), 8.32 (s, 1 H), 8.03 (s, 2 H), 7.77 (d, *J* = 8.4 Hz, 1 H), 7.72 (d, *J* = 8.4 Hz, 1 H), 7.64 (s, 1 H), 7.60–7.58 (m, 1 H), 7.42 (d, *J* = 8.4 Hz, 1 H), 7.37 (d, *J* = 8.4 Hz, 1 H), 5.08 (s, 2 H), 2.39 (s, 3 H); <sup>13</sup>C NMR (150 MHz, DMSO-*d*<sub>6</sub>) δ 167.2, 164.6, 163.5, 153.4, 149.1, 142.4, 140.3, 137.5, 137.3, 136.1, 133.3, 131.3, 131.2, 129.8, 127.9, 125.7, 124.5, 123.1, 122.9, 122.7, 118.9, 117.1, 115.8, 105.7, 54.7, 18.6. MS (ESI) *m/z* 520.3 for [M+H]<sup>+</sup>. HRMS (ESI) *m/z* calculated for C<sub>26</sub>H<sub>21</sub>F<sub>3</sub>N<sub>7</sub>O<sub>2</sub> [M+H]<sup>+</sup> 520.1709, found 520.1696. HPLC purity 98.0% (MeOH: H<sub>2</sub>O = 80 : 20, 1.0 mL/min, t<sub>R</sub> = 3.76 min).

4.1.6.4. 1-Methyl-*N*-(6-(1-(2-((4-methyl-3-(trifluoromethyl)phenyl)amino)-2-oxoethyl)-1H-pyrazol-4-yl)-1H-indazol-3-yl)-1H-pyrazole-4-carboxamide (**W18**). White solid powder; yield 84%; m.p.: 271–273 °C; <sup>1</sup>H NMR (600 MHz, DMSO-*d*<sub>6</sub>) δ 12.69 (s, 1 H), 10.63 (s, 1 H), 10.42 (s, 1 H), 8.36 (s, 1 H), 8.31 (s, 1 H), 8.09 (s, 1 H), 8.04 (s, 1 H), 8.02 (s, 1 H), 7.75 (d, *J* = 8.4 Hz, 1 H), 7.72 (d, *J* = 7.8 Hz, 1 H), 7.61 (s, 1 H), 7.42 (d, *J* = 8.4 Hz, 1 H), 7.33 (d, *J* = 9.0 Hz, 1 H), 5.08 (s, 2 H), 3.91 (s, 3 H), 2.39 (s, 3 H); <sup>13</sup>C NMR (150 MHz, DMSO-*d*<sub>6</sub>) δ 166.3, 161.0, 142.4, 140.7, 139.7, 137.5, 137.3, 133.4, 133.3, 131.2, 129.8, 128.1, 127.9, 125.7, 124.3, 123.3, 123.1, 122.8, 118.6, 118.3, 116.6, 115.9, 105.6, 55.2, 18.6. MS (ESI) *m/z* 523.3 for [M+H]<sup>+</sup>. HRMS (ESI) *m/z* calculated for C<sub>25</sub>H<sub>22</sub>F<sub>3</sub>N<sub>8</sub>O<sub>2</sub> [M+H]<sup>+</sup> 523.1818, found 523.1802. HPLC purity 99.2% (MeOH: H<sub>2</sub>O = 80 : 20, 1.0 mL/min, t<sub>R</sub> = 3.33 min).

4.1.6.5. 2-(4-(3-(ethylamino)-1H-indazol-6-yl)-1H-pyrazol-1-yl)-*N*-(4-methyl-3-(trifluoromethyl)phenyl)acetamide (**W19**). White solid

powder; yield 43%; m.p.: 238–240 °C;  $^1\text{H}$  NMR (600 MHz, DMSO- $d_6$ )  $\delta$  11.52 (s, 1 H), 10.70 (s, 1 H), 8.26 (s, 1 H), 8.03 (s, 1 H), 7.98 (s, 1 H), 7.72–7.69 (m, 2 H), 7.42–7.40 (m, 2 H), 7.21 (d,  $J = 8.4$  Hz, 1 H), 5.07 (s, 2 H), 3.31 (q,  $J = 7.2$  Hz, 2 H), 2.39 (s, 3 H), 1.25 (t,  $J = 7.2$  Hz, 3 H);  $^{13}\text{C}$  NMR (150 MHz, DMSO- $d_6$ )  $\delta$  166.3, 150.3, 143.1, 137.5, 137.3, 133.3, 131.6, 131.2, 129.6, 128.1, 127.9, 125.7, 123.9, 123.0, 121.2, 116.7, 112.7, 105.2, 55.8, 38.3, 18.6, 15.3. MS (ESI)  $m/z$  443.3 for  $[\text{M}+\text{H}]^+$ . HRMS (ESI)  $m/z$  calculated for  $\text{C}_{22}\text{H}_{22}\text{F}_3\text{N}_6\text{O}$   $[\text{M}+\text{H}]^+$  443.1807, found 443.1792. HPLC purity 99.5% (MeOH:  $\text{H}_2\text{O} = 80 : 20$ , 1.0 mL/min,  $t_{\text{R}} = 3.76$  min).

4.1.6.6. 2-(4-(3-((cyclopropylmethyl)amino)-1H-indazol-6-yl)-1H-pyrazol-1-yl)-N-(4-methyl-3-(trifluoromethyl)phenyl)acetamide (**W20**). White solid powder; yield 48%; m.p.: 214–216 °C;  $^1\text{H}$  NMR (600 MHz, DMSO- $d_6$ )  $\delta$  11.33 (s, 1 H), 10.60 (s, 1 H), 8.24 (s, 1 H), 8.03 (s, 1 H), 7.96 (s, 1 H), 7.73–7.69 (m, 2 H), 7.42 (d,  $J = 8.4$  Hz, 1 H), 7.38 (s, 1 H), 7.17 (d,  $J = 8.4$  Hz, 1 H), 5.06 (s, 2 H), 3.13 (d,  $J = 7.2$  Hz, 2 H), 2.38 (s, 3 H), 1.19–1.15 (m, 1 H), 0.47–0.45 (m, 2 H), 0.25–0.24 (m, 2 H);  $^{13}\text{C}$  NMR (150 MHz, DMSO- $d_6$ )  $\delta$  166.3, 150.6, 143.0, 137.4, 137.3, 133.3, 131.2, 131.1, 129.5, 127.9, 125.7, 123.9, 123.2, 123.1, 121.1, 116.3, 112.9, 105.1, 55.2, 47.7, 18.6, 12.3, 4.0. MS (ESI)  $m/z$  469.3 for  $[\text{M}+\text{H}]^+$ . HRMS (ESI)  $m/z$  calculated for  $\text{C}_{24}\text{H}_{24}\text{F}_3\text{N}_6\text{O}$   $[\text{M}+\text{H}]^+$  469.1964, found 469.1947. HPLC purity 97.5% (MeOH:  $\text{H}_2\text{O} = 80 : 20$ , 1.0 mL/min,  $t_{\text{R}} = 3.74$  min).

#### 4.1.7. General procedure for the synthesis of target compounds **W21–22**

To a suspension of compound **21a** or **21b** (0.2 mmol, 1.0 eq) in tetrahydrofuran (4 mL) was added cyclopropane carbonyl chloride (2.5 eq) followed by DIEA (4.8 eq). The reaction condition and post-treatment method were the same as compound **W13**. The final residue was purified by silica gel flash chromatography (DCM: MeOH = 100:1–10:1) to obtain target compounds **W21–22**.

4.1.7.1. *N*-(6-(3-methyl-1-(2-((4-methyl-3-(trifluoromethyl)phenyl)amino)-2-oxoethyl)yl)-1H-pyrazol-4-yl)-1H-indazol-3-yl)cyclopropanecarboxamide (**W21**). Pale pink solid powder; yield 47%; m.p.: 240–242 °C;  $^1\text{H}$  NMR (600 MHz, DMSO- $d_6$ )  $\delta$  12.54 (s, 1 H), 10.65–10.63 (m, 2 H), 8.03 (s, 1 H), 7.78 (d,  $J = 8.4$  Hz, 1 H), 7.69–7.68 (m, 2 H), 7.40–7.39 (m, 2 H), 7.12 (s, 1 H), 5.06 (s, 1 H), 4.97 (s, 1 H), 2.38 (s, 3 H), 2.34 (s, 3 H), 1.92 (s, 1 H), 0.84 (s, 4 H);  $^{13}\text{C}$  NMR (150 MHz, DMSO- $d_6$ )  $\delta$  172.2, 166.4, 145.3, 142.2, 140.9, 138.2, 137.3, 136.9, 133.3, 131.5, 131.2, 127.9, 125.7, 123.9, 123.4, 123.0, 120.4, 116.6, 107.4, 54.8, 18.6, 13.9, 10.8, 7.7. MS (ESI)  $m/z$  497.3 for  $[\text{M}+\text{H}]^+$ . HRMS (ESI)  $m/z$  calculated for  $\text{C}_{25}\text{H}_{24}\text{F}_3\text{N}_6\text{O}_2$   $[\text{M}+\text{H}]^+$  497.1913, found 497.1897. HPLC purity 99.7% (MeOH:  $\text{H}_2\text{O} = 80 : 20$ , 1.0 mL/min,  $t_{\text{R}} = 3.82$  min).

4.1.7.2. *N*-(6-(3,5-dimethyl-1-(2-((4-methyl-3-(trifluoromethyl)phenyl)amino)-2-oxoethyl)yl)-1H-pyrazol-4-yl)-1H-indazol-3-yl)cyclopropanecarboxamide (**W22**). Yellow solid powder; yield 64%; m.p.: 237–238 °C;  $^1\text{H}$  NMR (600 MHz, DMSO- $d_6$ )  $\delta$  12.57 (s, 1 H), 10.67 (s, 1 H), 10.62 (s, 1 H), 8.06 (s, 1 H), 7.80 (d,  $J = 7.8$  Hz, 1 H), 7.70 (d,  $J = 9.0$  Hz, 1 H), 7.42 (d,  $J = 7.8$  Hz, 1 H), 7.23 (s, 1 H), 6.97 (d,  $J = 8.4$  Hz, 1 H), 4.97 (s, 2 H), 2.40 (s, 3 H), 2.27 (s, 3 H), 2.17 (s, 3 H), 1.94 (s, 1 H), 0.85–0.83 (m, 4 H);  $^{13}\text{C}$  NMR (150 MHz, DMSO- $d_6$ )  $\delta$  172.3, 166.6, 145.0, 142.0, 140.9, 137.9, 137.3, 133.3, 132.4, 131.2, 127.9, 125.7, 123.9, 123.0, 121.9, 119.0, 116.6, 115.1, 110.0, 52.5, 18.7, 14.1, 13.0, 10.5, 7.7. MS (ESI)  $m/z$  511.3 for  $[\text{M}+\text{H}]^+$ . HRMS (ESI)  $m/z$  calculated for  $\text{C}_{26}\text{H}_{26}\text{F}_3\text{N}_6\text{O}_2$   $[\text{M}+\text{H}]^+$  511.2069, found 511.2057. HPLC purity 99.6% (MeOH:  $\text{H}_2\text{O} = 80 : 20$ , 1.0 mL/min,  $t_{\text{R}} = 3.86$  min).

#### 4.1.8. General procedure for the synthesis of compounds **24** and **27a–b**

To a mixture of compounds **23** or **26a–b** (2.1 mmol, 1.0 eq), bis(pinacolato)diboron (1.4 eq), Pd(dppf)Cl<sub>2</sub> (0.1 eq) and potassium acetate (3.0 eq) in anhydrous 1,4-dioxane (10 mL) was heated to reflux for 12 h under argon. After reactant consumed completely, the reaction solution was filtered through a pad of Celite and rinsed with ethyl acetate, and the filtrate was concentrated in vacuo. The residue was purified by column chromatography (PE: EtOAc = 50:1–6:1) to afford compounds **24** and **27a–b**.

4.1.8.1. *N*-(4-methyl-3-(trifluoromethyl)phenyl)-2-(5-(4,4,5,5-tetramethyl-1,3,2-dioxaborolan-2-yl)thiophen-2-yl)acetamide (**24**). Yellow liquid; yield 58%;  $^1\text{H}$  NMR (600 MHz, CDCl<sub>3</sub>)  $\delta$  7.60–7.59 (m, 3 H), 7.31 (s, 1 H), 7.22 (d,  $J = 7.8$  Hz, 1 H), 7.12 (s, 1 H), 3.99 (s, 2 H), 2.42 (s, 3 H), 1.35 (s, 12 H).

4.1.8.2. *N*-(4-methyl-3-(trifluoromethyl)phenyl)-2-(3-(4,4,5,5-tetramethyl-1,3,2-dioxaborolan-2-yl)phenyl)acetamide (**27a**). White solid powder; yield >99%;  $^1\text{H}$  NMR (600 MHz, CDCl<sub>3</sub>)  $\delta$  7.79 (d,  $J = 6.6$  Hz, 1 H), 7.76 (s, 1 H), 7.60–7.58 (m, 2 H), 7.45–7.42 (m, 2 H), 7.32 (s, 1 H), 7.19 (d,  $J = 8.4$  Hz, 1 H), 3.74 (s, 2 H), 2.41 (s, 3 H), 1.36 (s, 12 H).

4.1.8.3. *N*-(4-methyl-3-(trifluoromethyl)phenyl)-2-(4-(4,4,5,5-tetramethyl-1,3,2-dioxaborolan-2-yl)phenyl)acetamide (**27b**). White solid powder; yield >99%;  $^1\text{H}$  NMR (600 MHz, CDCl<sub>3</sub>)  $\delta$  7.86 (d,  $J = 7.8$  Hz, 2 H), 7.56–7.55 (m, 2 H), 7.35 (d,  $J = 7.8$  Hz, 2 H), 7.19 (d,  $J = 7.8$  Hz, 1 H), 7.06 (s, 1 H), 3.77 (s, 2 H), 2.41 (s, 3 H), 1.36 (s, 12 H).

#### 4.1.9. General procedure for the synthesis of target compounds **W23–25**

To a mixture of compound **12** (1.0 mmol, 1.0 eq), compound **24** or **27a–b** (1.3 eq) and Pd(dppf)Cl<sub>2</sub>·CH<sub>2</sub>Cl<sub>2</sub> (0.1 eq) in 1,4-dioxane (4.0 mL) was added 2 M Na<sub>2</sub>CO<sub>3</sub> aq (0.4 mL) and purged with argon. The resulting mixture was refluxed for 3 h. The reaction mixture was filtered and filtrate was evaporated in vacuo, the crude product was further purified by column chromatography (DCM: MeOH = 100:1–20:1) to obtain target compounds **W23–25**.

4.1.9.1. *N*-(6-(5-(2-((4-methyl-3-(trifluoromethyl)phenyl)amino)-2-oxoethyl)thiophen-2-yl)-1H-indazol-3-yl)cyclopropanecarboxamide (**W23**). Yellow solid powder; yield 32%; m.p.: 234–236 °C;  $^1\text{H}$  NMR (600 MHz, DMSO- $d_6$ )  $\delta$  12.65 (s, 1 H), 10.70 (s, 1 H), 10.50 (s, 1 H), 8.03 (s, 1 H), 7.81 (d,  $J = 9.0$  Hz, 1 H), 7.72 (d,  $J = 8.4$  Hz, 1 H), 7.56 (s, 1 H), 7.44 (d,  $J = 3.6$  Hz, 1 H), 7.40 (d,  $J = 8.4$  Hz, 1 H), 7.32 (d,  $J = 9.0$  Hz, 1 H), 7.02 (d,  $J = 3.6$  Hz, 1 H), 3.92 (s, 2 H), 2.39 (s, 3 H), 1.93 (s, 1 H), 0.85–0.82 (m, 4 H);  $^{13}\text{C}$  NMR (150 MHz, DMSO- $d_6$ )  $\delta$  172.2, 168.7, 143.2, 142.0, 141.1, 137.7, 137.2, 133.2, 132.5, 130.9, 128.4, 127.9, 125.8, 124.1, 123.9, 123.0, 118.2, 116.6, 105.9, 38.3, 18.6, 14.1, 7.7. MS (ESI)  $m/z$  499.2 for  $[\text{M}+\text{H}]^+$ . HRMS (ESI)  $m/z$  calculated for  $\text{C}_{25}\text{H}_{22}\text{F}_3\text{N}_4\text{O}_2\text{S}$   $[\text{M}+\text{H}]^+$  499.1416, found 499.1401. HPLC purity 99.7% (MeOH:  $\text{H}_2\text{O} = 80 : 20$ , 1.0 mL/min,  $t_{\text{R}} = 3.93$  min).

4.1.9.2. *N*-(6-(3-(2-((4-methyl-3-(trifluoromethyl)phenyl)amino)-2-oxoethyl)phenyl)-1H-indazol-3-yl)cyclopropanecarboxamide (**W24**). Pale yellow solid powder; yield 28%; m.p.: 163–165 °C;  $^1\text{H}$  NMR (600 MHz, DMSO- $d_6$ )  $\delta$  12.69 (s, 1 H), 10.71 (s, 1 H), 10.45 (s, 1 H), 8.02 (s, 1 H), 7.87 (d,  $J = 8.4$  Hz, 1 H), 7.71–7.68 (m, 2 H), 7.59–7.54 (m, 2 H), 7.45–7.42 (m, 1 H), 7.36–7.31 (m, 3 H), 3.74 (s, 2 H), 2.36 (s, 3 H), 1.93 (s, 1 H), 0.86 (s, 4 H);  $^{13}\text{C}$  NMR (150 MHz, DMSO- $d_6$ )  $\delta$  172.8, 169.9, 142.2, 141.0, 140.9, 139.0, 137.9, 136.8, 133.1, 130.7, 129.4, 128.8, 128.6, 128.0, 126.0, 123.7, 122.9, 120.1, 116.5, 115.9, 108.0, 43.8, 18.6, 14.1, 7.3. MS (ESI)  $m/z$  493.3 for  $[\text{M}+\text{H}]^+$ . HRMS

(ESI)  $m/z$  calculated for  $C_{27}H_{24}F_3N_4O_2$   $[M+H]^+$  493.1851, found 493.1835. HPLC purity 99.7% (MeOH:  $H_2O = 80 : 20$ , 1.0 mL/min,  $t_R = 3.95$  min).

4.1.9.3. *N*-(6-(4-(2-((4-methyl-3-(trifluoromethyl)phenyl)amino)-2-oxoethyl)phenyl)-1H-indazol-3-yl)cyclopropanecarboxamide (**W25**). White solid powder; yield 45%; m.p.: 289–291 °C;  $^1H$  NMR (600 MHz,  $DMSO-d_6$ )  $\delta$  12.68 (s, 1 H), 10.70 (s, 1 H), 10.48 (s, 1 H), 8.03 (s, 1 H), 7.84 (d,  $J = 7.8$  Hz, 1 H), 7.72 (d,  $J = 7.8$  Hz, 1 H), 7.67 (d,  $J = 7.2$  Hz, 2 H), 7.58 (s, 1 H), 7.44 (d,  $J = 7.8$  Hz, 2 H), 7.37 (d,  $J = 9.0$  Hz, 1 H), 7.32 (d,  $J = 8.4$  Hz, 1 H), 3.70 (s, 2 H), 2.36 (s, 3 H), 1.93 (s, 1 H), 0.84–0.81 (m, 4 H);  $^{13}C$  NMR (150 MHz,  $DMSO-d_6$ )  $\delta$  172.2, 169.9, 142.2, 140.9, 139.4, 138.9, 137.9, 135.5, 133.1, 130.7, 130.2, 128.0, 127.6, 125.8, 123.6, 122.9, 119.4, 116.5, 115.8, 107.8, 43.4, 18.6, 14.1, 7.7. MS (ESI)  $m/z$  493.3 for  $[M+H]^+$ . HRMS (ESI)  $m/z$  calculated for  $C_{27}H_{24}F_3N_4O_2$   $[M+H]^+$  493.1851, found 493.1837. HPLC purity 97.5% (MeOH:  $H_2O = 80 : 20$ , 1.0 mL/min,  $t_R = 3.93$  min).

4.1.10. Compound **W26** was prepared following the synthetic procedure of **W13**

To a suspension of compound **30** (0.36 mmol, 1.0 eq) in tetrahydrofuran (4 mL) was added cyclopropane carbonyl chloride (2.4 eq) followed by DIEA (4.8 eq). The reaction condition and post-treatment method were the same as compound **W13**. The final residue was recrystallized from isopropanol and dried in vacuum to obtain target compound **W26**.

4.1.10.1. *N*-(6-(1-(2-((4-methyl-3-(trifluoromethyl)phenyl)amino)-2-oxoethyl)-1H-1,2,3-triazol-4-yl)-1H-indazol-3-yl)cyclopropanecarboxamide (**W26**). White solid powder; yield 83%; m.p.: >300 °C;  $^1H$  NMR (600 MHz,  $DMSO-d_6$ )  $\delta$  12.54 (s, 1 H), 10.80 (s, 1 H), 10.55 (s, 1 H), 8.69 (s, 1 H), 8.03 (s, 1 H), 7.92 (s, 1 H), 7.87 (d,  $J = 8.4$  Hz, 1 H), 7.71 (d,  $J = 8.4$  Hz, 1 H), 7.55 (d,  $J = 8.4$  Hz, 1 H), 7.43 (d,  $J = 8.4$  Hz, 1 H), 5.42 (s, 2 H), 2.40 (s, 3 H), 1.93–1.91 (m, 1 H), 0.88–0.82 (m, 4 H);  $^{13}C$  NMR (150 MHz,  $DMSO-d_6$ )  $\delta$  171.6, 165.1, 147.0, 141.9, 140.5, 137.1, 133.4, 131.4, 129.8, 129.7, 128.2, 128.0, 125.7, 123.9, 123.1, 117.9, 116.7, 106.2, 52.8, 26.3, 18.6, 14.1, 7.7. MS (ESI)  $m/z$  484.3 for  $[M+H]^+$ . HRMS (ESI)  $m/z$  calculated for  $C_{23}H_{21}F_3N_7O_2$   $[M+H]^+$  484.1709, found 484.1694. HPLC purity 95.2% (MeOH:  $H_2O = 80 : 20$ , 1.0 mL/min,  $t_R = 3.67$  min).

## 4.2. Biological evaluation

### 4.2.1. Cell lines and cell culture

All the cell lines were obtained from the Shanghai Qishi Biotechnology Co., Ltd. (Shanghai, CHINA). Colon (HT-29) cells were grown in Dulbecco's modified Eagle's medium (DMEM/F-12, Gibco) whereas lung (A549), liver (HepG2) and gastric (HGC-27) cells were cultured in RPMI-1640 medium (Gibco). Human umbilical vein endothelial cells (HUVECs) and human gastric mucosal cells (GES-1) were cultured in endothelial cell medium (ECM) (ScienCell, SC-1001) with 1% endothelial cell growth supplement (ECGS) and DMEM medium, respectively. All the mediums were supplemented with 10% FBS (HyClone, GE Healthcare, Australia), 2%  $L$ -glutamine and 1% ampicillin/streptomycin, and incubated at 37 °C in a humidified atmosphere containing 5%  $CO_2$ . All synthesized compounds were prepared as 10 mM stock solutions for subsequent assay.

### 4.2.2. In vitro cytotoxicity evaluation

The cytotoxicity of the target compounds was measured *in vitro* using the MTT assay. Cells grown in the logarithmic phase were counted and seeded in 96-well cell culture plates ( $5 \times 10^3$  cells per well) for 24 h to allow attachment of cells to the wall of the plate.

Thereafter, cells were treated with different concentrations of compounds or positive control Sorafenib (Aladdin, Shanghai, CHINA) that dissolved in the medium and incubated at 37 °C for 72 h. Then, 10  $\mu$ L of MTT solution (5 mg/mL, Solarbio, Beijing, CHINA) was added to each well and the cells were further incubated for 4 h in dark at 37 °C. The unreacted MTT solution was removed and 100  $\mu$ L DMSO was added to each well to solubilise the produced formazan crystals. The absorbance of the solution at 490 nm was measured using a universal microplate reader (BIO-RAD, iMerk™, Japan), and each experiment was performed at least in triplicate. The  $IC_{50}$  values were determined from nonlinear regression analysis of the sigmoidal dose-response curve generated in Graph pad prism 5.0.

### 4.2.3. In vitro VEGFR-2 inhibition assay

The synthesized compounds were evaluated for their *in vitro* VEGFR-2 inhibitory activities using Caliper Mobility-Shift assay, which were carried out by Sundia (Shanghai, CHINA) MediTech Company, Ltd.. At first, 1  $\times$  kinase buffer was prepared and compounds were diluted to different final test concentrations and transferred 250 nL of above solution to assay plate by Echo550. Then 2.5  $\times$  protein solution using 1  $\times$  kinase buffer were prepared and 10  $\mu$ L of above solution was added to compound well and positive control well with negative control well for 10  $\mu$ L of 1  $\times$  kinase buffer, centrifuged at 1000 rpm for 30 s and incubated at room temperature for 10 min. At the same time, 5  $\times$  ATP and kinase substrate mixed solution with 1  $\times$  kinase buffer were prepared and 15  $\mu$ L of above solution was added to each well of the reaction plate. The mixture was centrifuged at 1000 rpm for 30 s and incubated at room temperature for 30 min. Next, 30  $\mu$ L of detection solution was added and the mixture was centrifuged at 1000 rpm for 30 s. Finally, the conversion rate was read by microplate reader (PerkinElmer, Caliper EZ Reader). Curve fitting was performed on Graphpad Prism 5.0 software to calculate  $IC_{50}$ .

### 4.2.4. Colony formation assay

HGC-27 cells in exponential growth phase were seeded into 6-well plates (500 cells/well) and incubated at 37 °C for 24 h. The culture medium was replaced with medium containing increasing concentrations (0.1, 0.5 and 1  $\mu$ M) of compound **W13**, compared with 0.1% DMSO (vehicle) and 5  $\mu$ M of Sorafenib (positive control), and incubated for 12 days. Then, the cells were washed with cold PBS, fixed with methanol and stained with 0.1% crystal violet solution for 30 min, respectively. The colonies (greater than 50 cells) were photographed.

### 4.2.5. Wound healing assay

HGC-27 cells were cultured in 6-well culture plates until the density reached to 80–90%. Cells were starved with serum-free medium for 12 h and followed by wounding with 200  $\mu$ L pipette tips to obtain 1 mm wide lanes per well. The cell debris was removed by washing with PBS and cells were supplied with 2 mL of complete medium (controls), complete medium containing different concentrations of compound **W13** (0.1, 0.5 and 1  $\mu$ M), and sorafenib (5  $\mu$ M). Images were captured after 0, 6, and 24 h with an inverted fluorescence microscope (Zeiss, VERT1, USA) and analyzed by Image J software.

### 4.2.6. Transwell migration assay

Initially, HGC-27 ( $1 \times 10^5$  cells) were suspended in 200  $\mu$ L of an FBS-free medium. The top chamber contained the vehicle and various concentrations of compound **W13** (0.1, 0.5 and 1  $\mu$ M) and sorafenib (5  $\mu$ M). The lower chamber was filled with 600  $\mu$ L of medium containing 10% FBS. After incubating at 37 °C for 24 h, the cells on the top side of the Transwell membrane were removed

with a cotton tip. The cells trapped on the bottom side of the membrane were fixed with methanol and stained with 0.1% crystal violet solution for 30 min, respectively. The migrated cells were then imaged with an inverted fluorescence microscope (Zeiss, VERT1, USA) and counted by Image J software for three independent fields randomly.

#### 4.2.7. Transwell invasion assay

The Transwell (12  $\mu\text{m}$  pore, Corning Incorporated) was pre-coated with 50  $\mu\text{L}$  Matrigel for 5 h at 37  $^{\circ}\text{C}$  to achieve solidification. HGC-27 cells were harvested and resuspended in serum-free medium containing 0, 0.1, 0.5 and 1  $\mu\text{M}$  of compound **W13** compared with 5  $\mu\text{M}$  of sorafenib, and added into the upper wells of the Transwell chamber at the density of  $5 \times 10^5$  cells/mL. While 600  $\mu\text{L}$  of RPMI-1640 containing 10% FBS was added into the lower chambers which had been coated with 50  $\mu\text{L}$  of Matrigel (1:8 dilution in serum-free medium, Corning/BD Biosciences). After 24 h of incubation at 37  $^{\circ}\text{C}$ , the invasion cells were fixed with methanol and stained with 0.1% crystal violet for 30 min, respectively. Then, the chambers were washed with PBS and left to dry. Images were photographed using an inverted fluorescence microscope (Zeiss, VERT1, USA) and counted by Image J software for three independent fields randomly.

#### 4.2.8. Apoptosis analysis

HGC-27 Cells were seeded in 60 mm Prtri dishes ( $1.0 \times 10^6$  cells/dish), incubated with 0.1% DMSO (vehicle), 5  $\mu\text{M}$  of Sorafenib (positive control) and different concentrations (0.1, 0.5 and 1  $\mu\text{M}$ ) of compound **W13** in the separately prepared medium for 24 h, respectively. After incubation, cells were harvested and incubated with 5  $\mu\text{L}$  of Annexin-V/FITC (YEASEN, CHINA) in binding buffer (10 mM HEPES, 140 mM NaCl, and 2.5 mM  $\text{CaCl}_2$  at pH 7.4) at room temperature for 15 min. PI solution was then added to the medium for another 10 min incubation. Almost 10 000 events were collected for each sample and analyzed by flow cytometry (BD, LSRFortessa, USA).

#### 4.2.9. Effect on ROS generation in HGC-27 cells

The intracellular ROS levels in HGC-27 cells were determined by CM-H<sub>2</sub>DCFDA staining. In this assay, HGC-27 cells were seeded in 6-well culture plates ( $5.0 \times 10^5$  cells/well) and incubated with various concentrations of compound **W13** (0.1, 0.5 and 1  $\mu\text{M}$ ) compared with 0.1% DMSO (vehicle) and 5  $\mu\text{M}$  of Sorafenib (positive control). After incubation for 24 h, the cells were harvested and stained with a 10  $\mu\text{M}$  solution of DCFH-DA in PBS for 20 min at 37  $^{\circ}\text{C}$ . The intensity of the green fluorescence was analyzed using flow cytometry.

#### 4.2.10. Western blot analysis

HUVECs and HGC-27 cells were seeded in 60 mm Prtri dishes ( $1.0 \times 10^6$  cells/dish) and incubated with 0.1% DMSO (vehicle), positive control Sorafenib (10  $\mu\text{M}$  for HUVEC; 5  $\mu\text{M}$  for HGC-27), and various concentrations of compound **W13** (1, 5 and 10  $\mu\text{M}$  for HUVEC; 0.1, 0.5 and 1  $\mu\text{M}$  for HGC-27), respectively. After incubation for 24 h, the cells were collected by centrifugation and washed twice with PBS chilled to 0  $^{\circ}\text{C}$ . Then, the cells were homogenized in RIPA lysis buffer containing 150 mM NaCl, 50 mM Tris (pH 7.4), 1% (w/v) sodium deoxycholate, 1% (v/v) Triton X-100, 0.1% (w/v) SDS, and 1 mM EDTA (Beyotime, CHINA) and 1% PMSF, 1% mixed phosphatase inhibitor (Solarbio, CHINA). The lysates were incubated on ice for 30 min, intermittently vortexed every 5 min, and centrifuged at 12 500 rpm for 15 min to harvest the supernatants. Next, the protein concentrations were determined by a BCA Protein Assay Kit (Solarbio, CHINA). The protein extracts were reconstituted in loading buffer containing 62 mM Tris-HCl, 2% SDS, 10% glycerol and

5%  $\beta$ -mercaptoethanol (Beyotime, CHINA), and the mixture was boiled at 100  $^{\circ}\text{C}$  for 15 min. An equal amount of the proteins (50 mg) were separated by 8–12% sodium dodecyl sulfate-polyacrylamide gel electrophoresis (SDS-PAGE) and transferred to nitrocellulose membranes (Amersham Biosciences, Little Chalfont, Buckinghamshire, UK). Then, the membranes were blocked with 5% nonfat dried milk in TBS containing 1% Tween-20 for 2 h at room temperature and were incubated overnight with specific primary antibodies (CST, USA) at 4  $^{\circ}\text{C}$ . After three washes in TBST, the membranes were incubated with the appropriate HRP-conjugated secondary antibodies at room temperature for 2 h. The blots were developed with enhanced chemiluminescence (YEASEN, CHINA) and were detected by an Tanon5200 imager (YPHBIO, CHINA). Each experiment was performed at least in triplicate and analyzed by Image J software.

#### 4.2.11. HUVECs tube formation assay

BD Matrigel™ (BD Bio-science, Heidelberg Germany) was thawed at 4  $^{\circ}\text{C}$  overnight prior. The 96-well plate was placed on ice prior to the coating and 50  $\mu\text{L}$  of matrigel was slowly added to each well with constant, gentle agitation for an even layer formation. The Matrigel was polymerized for 1 h at 37  $^{\circ}\text{C}$  and 100  $\mu\text{L}$  of HUVECs suspension ( $4 \times 10^5$  cells/mL) was added to each well. Subsequently, the cells were cultured with 0.1% DMSO (vehicle), 10  $\mu\text{M}$  of Sorafenib (positive control) and various concentrations (1, 5 and 10  $\mu\text{M}$ ) of compound **W13**, respectively, and added 20 ng/mL VEGF to each well incubating at 37  $^{\circ}\text{C}$  for 12 h. The tube formation was observed with an inverted fluorescence microscope (Zeiss, VERT1, USA) and photographed using ZEN 2.3 software. The corresponding area was measured as the number of pixels using Image J software.

### 4.3. Molecular docking studies

Molecular docking simulation was performed using the Glide module of Schrödinger. The ligands **W18** and sorafenib were prepared firstly using the Ligand Preparation module in Schrödinger, respectively. The X-ray crystallographic structures of VEGFR-2 (PDB ID: 3EWH) in DFG-out inactive conformation was downloaded from RCSB Protein Data Bank. The protein was filled in missing side chain and loops using Prime, removed the water molecule and minimized using the Protein Preparation Wizard module in the Schrödinger. Then, a grid was selected at the active site of the prepared protein structure using the Grid Generation module of Schrödinger and preserved the protein file. The Glide Docking module of Schrödinger was used to investigate the interactions between the synthesized compounds and VEGFR-2 after importing ligand files. All the figures illustrating the molecular docking results were visualized and generated using the Pymol software.

### Declaration of competing interest

The authors declare that they have no known competing financial interests or personal relationships that could have appeared to influence the work reported in this paper.

### Acknowledgments

This work was financially supported by the National Natural Science Foundation of China (NO. 21672093).

### Appendix A. Supplementary data

Supplementary data to this article can be found online at <https://doi.org/10.1016/j.ejmech.2021.113192>.

## References

- [1] P. Carmeliet, Angiogenesis in health and disease, *Nat. Med.* 9 (2003) 653–660.
- [2] S.M. Weis, D.A. Cheresh, Tumor angiogenesis: molecular pathways and therapeutic targets, *Nat. Med.* 17 (2011) 1359–1370.
- [3] K. Holmes, O.L. Roberts, A.M. Thomas, M.J. Cross, Vascular endothelial growth factor receptor-2: structure, function, intracellular signalling and therapeutic inhibition, *Cell. Signal.* 19 (2007) 2003–2012.
- [4] M. Akagi, M. Kawaguchi, W. Liu, M.F. McCarty, A. Takeda, F. Fan, O. Stoeltzing, A.A. Parikh, Y.D. Jung, C.D. Bucana, P.F. Mansfield, D.J. Hicklin, L.M. Ellis, Induction of neuropilin-1 and vascular endothelial growth factor by epidermal growth factor in human gastric cancer cells, *Brit. J. Canc.* 88 (2003) 796–802.
- [5] H.L. Goel, A.M. Mercurio, VEGF targets the tumour cell, *Nat. Rev. Canc.* 13 (2013) 871–882.
- [6] R.T.P. Poon, S.T. Fan, J. Wong, Clinical implications of circulating angiogenic factors in cancer patients, *J. Clin. Oncol.* 19 (2001) 1207–1225.
- [7] R.T.P. Poon, I.O.L. Ng, C. Lau, L.X. Zhu, W.C. Yu, C.M. Lo, S.T. Fan, J. Wong, Serum vascular endothelial growth factor predicts venous invasion in hepatocellular carcinoma: a prospective study, *Ann. Surg.* 233 (2001) 227–235.
- [8] N. Ferrara, A.P. Adams, Ten years of anti-vascular endothelial growth factor therapy, *Nat. Rev. Drug Discov.* 15 (2016) 385–403.
- [9] C. Fontanella, E. Ongaro, S. Bolzonello, M. Guardascione, G. Fasola, G. Aprile, Clinical advances in the development of novel VEGFR2 inhibitors, *Ann. Transl. Med.* 2 (2014) 123.
- [10] F. Musumeci, M. Radi, C. Brullo, S. Schenone, Vascular endothelial growth factor (VEGF) receptors: drugs and new inhibitors, *J. Med. Chem.* 55 (2012) 10797–10822.
- [11] F.-W. Peng, D.-K. Liu, Q.-W. Zhang, Y.-G. Xu, L. Shi, VEGFR-2 inhibitors and the therapeutic applications thereof: a patent review (2012–2016), *Expert Opin. Ther. Pat.* 27 (2017) 987–1004.
- [12] R.S.K. Vijayan, P. He, V. Modi, K.C. Duong-Ly, H. Ma, J.R. Peterson, R.L. Dunbrack Jr., R.M. Levy, Conformational analysis of the DFG-Out kinase motif and biochemical profiling of structurally validated type II inhibitors, *J. Med. Chem.* 58 (2015) 466–479.
- [13] P.A. Harris, A. Bolor, M. Cheung, R. Kumar, R.M. Crosby, R.G. Davis-Ward, A.H. Epperly, K.W. Hinkle, R.N. Hunter III, J.H. Johnson, V.B. Knick, C.P. Laudeman, D.K. Luttrell, R.A. Mook, R.T. Nolte, S.K. Rudolph, J.R. Szewczyk, A.T. Truesdale, J.M. Veal, L. Wang, J.A. Stafford, Discovery of 5-(4-(2,3-dimethyl-2H-indazol-6-yl)methylamino-2-pyrimidinyl-amino-2-methylbenzenesulfonamide (pazopanib), a novel and potent vascular endothelial growth factor receptor inhibitor, *J. Med. Chem.* 51 (2008) 4632–4640.
- [14] D.D. Hu-Lowe, H.Y. Zou, M.L. Grazzini, M.E. Hallin, G.R. Wickman, K. Amundson, J.H. Chen, D.A. Rewolinski, S. Yamazaki, E.Y. Wu, M.A. McTigue, B.W. Murray, R.S. Kania, P. O'Connor, D.R. Shalinsky, S.L. Bender, Nonclinical antiangiogenesis and antitumor activities of axitinib (AG-013736), an oral, potent, and selective inhibitor of vascular endothelial growth factor receptor tyrosine kinases 1, 2, 3, *Clin. Canc. Res.* 14 (2008) 7272–7283.
- [15] R. Roskoski Jr., Sunitinib: a VEGF and PDGF receptor protein kinase and angiogenesis inhibitor, *Biochem. Biophys. Res. Commun.* 356 (2007) 323–328.
- [16] Y. Dai, K. Hartandi, Z. Ji, A.A. Ahmed, D.H. Albert, J.L. Bauch, J.J. Bouska, P.F. Bousquet, G.A. Cunha, K.B. Glaser, C.M. Harris, D. Hickman, J. Guo, J. Li, P.A. Marcotte, K.C. Marsh, M.D. Moskey, R.L. Martin, A.M. Olson, D.J. Osterling, L.J. Pease, N.B. Soni, K.D. Stewart, V.S. Stoll, P. Tapang, D.R. Reuter, S.K. Davidson, M.R. Michaelides, Discovery of N-(4-(3-amino-1H-indazol-4-yl)phenyl)-N'-(2-fluoro-5-methylphenyl)urea (ABT-869), a 3-aminoindazole-based orally active multitargeted receptor tyrosine kinase inhibitor, *J. Med. Chem.* 50 (2007) 1584–1597.
- [17] S. Qin, Phase III study of apatinib in advanced gastric cancer: a randomized, double-blind, placebo-controlled trial, *J. Clin. Oncol.* 32 (2014) 4003–4003.
- [18] S. Wilhelm, C. Carter, M. Lynch, T. Lowinger, J. Dumas, R.A. Smith, B. Schwartz, R. Simantov, S. Kelley, Discovery and development of sorafenib: a multitargeted inhibitor for treating cancer, *Nat. Rev. Drug Discov.* 5 (2006) 835–844.
- [19] S.M. Wilhelm, C. Carter, L.Y. Tang, D. Wilkie, A. McNabola, H. Rong, C. Chen, X.M. Zhang, P. Vincent, M. McHugh, Y.C. Cao, J. Shujath, S. Gawlak, D. Eveleigh, B. Rowley, L. Liu, L. Adnane, M. Lynch, D. Auclair, I. Taylor, R. Gedrich, A. Voznesensky, B. Riedl, L.E. Post, G. Bollag, P.A. Trail, BAY 43-9006 exhibits broad spectrum oral antitumor activity and targets the RAF/MEK/ERK pathway and receptor tyrosine kinases involved in tumor progression and angiogenesis, *Canc. Res.* 64 (2004) 7099–7109.
- [20] A. Leonetti, M. Bersanelli, B. Castagneto, C. Masini, G. Di Meglio, B. Pellegrino, S. Buti, Outcome and safety of sorafenib in metastatic renal cell carcinoma dialysis patients: a systematic review, *Clin. Genitourin. Canc.* 14 (2016) 277–283.
- [21] C. Cainap, S. Qin, W.-T. Huang, I.J. Chung, H. Pan, Y. Cheng, M. Kudo, Y.-K. Kang, P.-J. Chen, H.-C. Toh, V. Gorbunova, F.A.L.M. Eskens, J. Qian, M.D. McKee, J.L. Ricker, D.M. Carlson, S. El-Nowiem, Linifanib versus sorafenib in patients with advanced hepatocellular carcinoma: results of a randomized phase III trial, *J. Clin. Oncol.* 33 (2015) 172–177.
- [22] M. Kudo, R.S. Finn, S. Qin, K.-H. Han, K. Ikeda, F. Piscaglia, A. Baron, J.-W. Park, G. Han, J. Jassem, J.F. Blanc, A. Vogel, D. Komov, T.R.J. Evans, C. Lopez, C. Dutcus, M. Guo, K. Saito, S. Kraljevic, T. Tamai, M. Ren, A.-L. Cheng, Lenvatinib versus sorafenib in first-line treatment of patients with unresectable hepatocellular carcinoma: a randomised phase 3 non-inferiority trial, *Lancet* 391 (2018) 1163–1173.
- [23] J.L. Raoula, M. Kudob, R.S. Finn, J. Edeline, M. Reige, Systemic therapy for intermediate and advanced hepatocellular carcinoma: sorafenib and beyond, *Canc. Treat. Rev.* 68 (2018) 16–24.
- [24] R.K. Jain, D.G. Duda, J.W. Clark, J.S. Loeffler, Lessons from phase III clinical trials on anti-VEGF therapy for cancer, *Nat. Clin. Pract. Oncol.* 3 (2006) 24–40.
- [25] A.-L. Cheng, Y.-K. Kang, Z. Chen, C.-J. Tsao, S. Qin, J.S. Kim, R. Luo, J. Feng, S. Ye, T.-S. Yang, J. Xu, Y. Sun, H. Liang, J. Liu, J. Wang, W.Y. Tak, H. Pan, K. Burack, J. Zou, D. Voliotis, Z. Guan, Efficacy and safety of sorafenib in patients in the Asia-Pacific region with advanced hepatocellular carcinoma: a phase III randomised, double-blind, placebo-controlled trial, *Lancet Oncol.* 10 (2009) 25–34.
- [26] S. Xia, Y. Pan, Y. Liang, J. Xu, X. Cai, The microenvironmental and metabolic aspects of sorafenib resistance in hepatocellular carcinoma, *EBioMedicine* 51 (2020) 102610.
- [27] Nielka P. van Erp, Hans Gelderblom, Henk-Jan Guchelaar, Clinical pharmacokinetics of tyrosine kinase inhibitors, *Canc. Treat. Rev.* 35 (2009) 692–706.
- [28] D.D. Gaikwad, A.D. Chaplikar, C.G. Devkate, K.D. Warad, A.P. Tayade, R.P. Pawar, A.J. Domb, Synthesis of indazole motifs and their medicinal importance: an overview, *Eur. J. Med. Chem.* 90 (2015) 707–731.
- [29] Z. Jiang, L. Wang, X. Liu, C. Chen, B. Wang, W. Wang, C. Hu, K. Yu, Z. Qi, Q. Liu, A. Wang, J. Liu, G. Hong, W. Wang, Q. Liu, Discovery of a highly selective VEGFR2 kinase inhibitor CHMFL-VEGR2-002 as a novel anti-angiogenesis agent, *Acta Pharm. Sin. B.* 10 (2020) 488–497.
- [30] Y. Zhang, Y. Chen, D. Zhang, L. Wang, T. Lu, Y. Jiao, Discovery of novel potent VEGFR-2 inhibitors exerting significant antiproliferative activity against cancer cell lines, *J. Med. Chem.* 61 (2018) 140–157.
- [31] Y.-X. Bo, R. Xiang, Y. Xu, S.-Y. Hao, X.-R. Wang, S.-W. Chen, Synthesis, biological evaluation and molecular modeling study of 2-amino-3,5-disubstituted-pyrazines as Aurora kinases inhibitors, *Bioorg. Med. Chem.* 28 (2020) 115351.
- [32] X. Deng, W. Zhou, E. Weisberg, J. Wang, J. Zhang, T. Sasaki, E. Nelson, J.D. Griffin, P.A. Jaenne, N.S. Gray, An amino-indazole scaffold with spectrum selective kinase inhibition of FLT3, PDGFR alpha and kit, *Bioorg. Med. Chem. Lett.* 22 (2012) 4579–4584.
- [33] J. Cui, X. Peng, D. Gao, Y. Dai, J. Ai, Y. Li, Optimization of 1H-indazol-3-amine derivatives as potent fibroblast growth factor receptor inhibitors, *Bioorg. Med. Chem. Lett.* 27 (2017) 3782–3786.
- [34] T. Fukuda, K. Ueda, T. Ishiyama, R. Goto, S. Muramatsu, M. Hashimoto, K. Watanabe, N. Tanaka, Synthesis and SAR studies of 3,6-disubstituted indazole derivatives as potent hepcidin production inhibitors, *Bioorg. Med. Chem. Lett.* 27 (2017) 2148–2152.
- [35] M.J. Stocks, S. Barber, R. Ford, F. Leroux, S. St-Gallay, S. Teague, Y.F. Xue, Structure-driven HTL: design and synthesis of novel aminoindazole inhibitors of c-Jun N-terminal kinase activity, *Bioorg. Med. Chem. Lett.* 15 (2005) 3459–3462.
- [36] Y. Li, Y. Xiong, G. Zhang, L. Zhang, W. Yang, J. Yang, L. Huang, Z. Qiao, Z. Miao, G. Lin, Q. Sun, T. Niu, L. Chen, D. Niu, L. Li, S. Yang, Identification of 5-(2,3-dihydro-1H-indol-5-yl)-7H-pyrrolo [2,3-d] pyrimidin-4-amine derivatives as a new class of receptor-interacting protein kinase 1 (RIPK1) inhibitors, which showed potent activity in a tumor metastasis model, *J. Med. Chem.* 61 (2018) 11398–11414.
- [37] C. Liu, H. Gao, T. Li, Y. Xiao, X. Cheng, Bisthiophene/triazole based 4,6-diamino-1,3,5-triazine triblock polyphiles: synthesis, self-assembly and metal binding properties, *J. Mol. Struct.* 1193 (2019) 294–302.
- [38] Z.-Y. Qi, S.-Y. Hao, H.-Z. Tian, H.-L. Bian, L. Hui, S.-W. Chen, Synthesis and biological evaluation of 1-(benzofuran-3-yl)-4-(3,4,5-trimethoxyphenyl)-1H-1,2,3-triazole derivatives as tubulin polymerization inhibitors, *Bioorg. Chem.* 94 (2020) 103392.
- [39] A.L. Hopkins, G.M. Keserue, P.D. Leeson, D.C. Rees, C.H. Reynolds, The role of ligand efficiency metrics in drug discovery, *Nat. Rev. Drug Discov.* 13 (2014) 105–121.
- [40] H.-J. Park, Y. Zhang, S.P. Georgescu, K.L. Johnson, D. Kong, J.B. Galper, Human umbilical vein endothelial cells and human dermal microvascular endothelial cells offer new insights into the relationship between lipid metabolism and angiogenesis, *Stem Cell Rev.* 2 (2006) 93–101.
- [41] M.A. Zeidan, A.S. Mostafa, R.M. Goma, L.A. Abou-zeid, M. El-Mesery, M.A.A. El-Sayed, K.B. Selim, Design, synthesis and docking study of novel picolinamide derivatives as anticancer agents and VEGFR-2 inhibitors, *Eur. J. Med. Chem.* 168 (2019) 315–329.
- [42] M.A. Aziz, R.A.T. Serya, D.S. Lasheen, A.K. Abdel-Aziz, A. Esmat, A.M. Mansour, A.N.B. Singab, K.A.M. Abouzid, Discovery of potent VEGFR-2 inhibitors based on furoprimidine and thienopyrimidine scaffolds as cancer targeting agents, *Sci. Rep. (U.K.)* 6 (2016) 24460.
- [43] S. Sana, V.G. Reddy, S. Bhandari, T.S. Reddy, R. Tokala, A.P. Sakla, S.K. Bhargava, N. Shankaraiah, Exploration of carbamide derived pyrimidine-thioindole conjugates as potential VEGFR-2 inhibitors with anti-angiogenesis effect, *Eur. J. Med. Chem.* 200 (2020) 112457.
- [44] P. Friedl, K. Wolf, Tumour-cell invasion and migration: diversity and escape mechanisms, *Nat. Rev. Canc.* 3 (2003) 362–374.
- [45] G. Cox, K.J. O'Byrne, Matrix metalloproteinases and cancer, *Anticancer Res.* 21 (2001) 4207–4219.
- [46] C.-Y. Loh, J.Y. Chai, T.F. Tang, W.F. Wong, G. Sethi, M.K. Shanmugam, P.P. Chong, C.Y. Looi, The E-cadherin and N-cadherin switch in epithelial-to-mesenchymal transition: signaling, therapeutic implications, and challenges, *Cells* 8 (2019) 1118.

- [47] W. Hu, J.J. Kavanagh, Anticancer therapy targeting the apoptotic pathway, *Lancet Oncol.* 4 (2003) 721–729.
- [48] J.M. Suski, M. Lebiezinska, M. Bonora, P. Pinton, J. Duszynski, M.R. Wieckowski, Relation between mitochondrial membrane potential and ROS formation, mitochondrial bioenergetics: methods and protocols, *Methods Mol. Biol.* (2012) 357–381.
- [49] S. Kikuchi, Y. Obata, K. Yagyu, Y. Lin, T. Nakajima, O. Kobayashi, M. Kikuichi, R. Ushijima, M. Kurosawa, J. Ueda, Reduced serum vascular endothelial growth factor receptor-2 (sVEGFR-2) and sVEGFR-1 levels in gastric cancer patients, *Canc. Sci.* 102 (2011) 866–869.
- [50] O. Tapia, I. Riquelme, P. Leal, A. Sandoval, S. Aedo, H. Weber, P. Letelier, E. Bellolio, M. Villaseca, P. Garcia, J. Carlos Roa, The PI3K/AKT/mTOR pathway is activated in gastric cancer with potential prognostic and predictive significance, *Virchows Arch.* 465 (2014) 25–33.
- [51] A.K. Olsson, A. Dimberg, J. Kreuger, L. Claesson-Welsh, VEGF receptor signalling-in control of vascular function, *Nat. Rev. Mol. Cell Biol.* 7 (2006) 359–371.
- [52] N. Ferrara, H.P. Gerber, J. LeCouter, The biology of VEGF and its receptors, *Nat. Med.* 9 (2003) 669–676.